Applied Catalysis B: Environmental 340 (2024) 123161

Contents lists available at ScienceDirect

Applied Catalysis B: Environmental

journal homepage: www.elsevier.com/locate/apcatb

Recent advances of ammonia synthesis under ambient conditions over metal-organic framework based electrocatalysts

Yu Yu [a,1], Yuan Li [a,1], Yu Fang [a], Lili Wen [b], Binbin Tu [b], Yi Huang [b,*]

[a] School of Chemistry and Chemical Engineering, Anhui University, Hefei 230601, PR China
[b] Key Laboratory of Pesticide & Chemical Biology of Ministry of Education, College of Chemistry, Central China Normal University, Wuhan 430079, PR China

ARTICLE INFO

Keywords:
Ammonia electrosynthesis
Electrocatalytic reduction reactions
Metal-organic frameworks (MOFs)
MOFs derivatives

ABSTRACT

Ammonia (NH_3) is an essential chemical and a promising fuel, but its industrially produced process is carbon-intensive and highly energy-consuming. Developing a green and sustainable NH_3 synthesis route is extremely urgent. Electrochemical ammonia synthesis (EAS) powered by renewable electricity energy under ambient conditions is fascinating, while exploring the efficient electrocatalysts and suitable nitrogen source is critical. Due to the unique characteristics of adjustable porosity and component, large specific surface area and diverse structure, metal-organic frameworks (MOFs) and their various derivatives have captured immense interest in EAS. Herein, the advance in EAS via electrocatalytic reduction reactions (ERRs) from various nitrogen source under ambient conditions over MOF-based electrocatalysts is timely summarized, aiming to offer a deep insight to the structure-activity relationship of MOF-based electrocatalysts for EAS. Current challenges and future prospects for EAS are proposed at the end of this review as well.

1. Introduction

Ammonia (NH_3) is a vital chemical in agricultural and industrial applications, such as fertilizer, pharmaceutical, and chemical production [1], as well as a potential hydrogen energy carrier due to the high hydrogen mass fraction (17.5 wt%), zero carbon content and much higher liquefaction temperature (−33 °C) [2,3], Currently, the global NH_3 production is close to 200 million metric tons, which highly relies on the traditional Haber-Bosch (H-B) process [4]. However, this process requires high temperature (300–500 °C) and high pressure (150–300 atm) to break the highly inert N≡N triple bond, which consumes 1 − 2% of worldwide energy consumption along with over 1% of the world's greenhouse gas emission [5–7]. Additionally, large and centralized plant infrastructure of H-B process limits the location of NH_3 plants. Thus, it is urgently needed to exploit a sustainable, distributed and environmentally friendly process as an alternative to the traditional H-B process.

Electrochemical ammonia synthesis (EAS) driven by the renewable electricity energy under ambient conditions is an attractive strategy for green NH_3 synthesis in small-scale devices [8–14]. Recently, many efforts have been made to synthesize NH_3 from abundant nitrogen (N_2) under aqueous conditions via electrocatalysis [15–19]. However, the yield of NH_3 is far from the demand of industrial requirements due to the poor water solubility and high bond energy (941 kJ mol^{-1}) of N_2 as well as the competitive hydrogen evolution reaction (HER) during the electrocatalytic process [20]. Some strategies have been adopted to improve the yield and selectivity of NH_3. For example, to avoid the dissolution issues of N_2 and competitive HER, a case in point is electrochemical lithium-mediated N_2 reduction reaction (Li-NRR) in nonaqueous electrolytes [21–23]. During the Li-NRR, Li^+ is first reduced to metallic Li, which then spontaneously reacts with N_2 to generate nitrogenous lithium compound; subsequently, the nitrogenous lithium compound is converted into NH_3 with proton sources through electrocatalysis [24]. Another promising strategy is developing oxynitrides (e.g., nitrate (NO_3^-), nitrite (NO_2^-) and gaseous nitrogen dioxides (NO_x)) as nitrogen source instead of N_2 due to the following reasons: 1) the lower N = O bond energy (204 kJ mol^{-1}) and higher solubility make it easier for the adsorption and activation of these oxynitrides than N_2, which can significantly increase the yield and selectivity of NH_3; 2) these oxynitrides as environmental pollutants are excessive in groundwater and atmosphere with the development of industry and agriculture, so that electrochemical conversion of these oxynitrides pollutants to high-value NH_3 can achieve "turn waste into wealth" [25–30]. Regardless of the

* Corresponding author.
E-mail address: yihuang@ccnu.edu.cn (Y. Huang).
[1] These authors contributed equally to this work.

https://doi.org/10.1016/j.apcatb.2023.123161
Received 5 June 2023; Received in revised form 19 July 2023; Accepted 8 August 2023
Available online 10 August 2023

development of the various strategies, efficient electrocatalysts are the core of EAS. Developing the advanced electrocatalytic materials with abundant active sites, good adsorption capacity and high stability for efficient and stable NH_3 synthesis is crucial but greatly challenging.

Metal-organic framework (MOF) is a class of crystalline organic-inorganic hybrid functional porous material, which is assembled by metal ions/clusters and organic linkers [31,32]. Due to their unique adjustable porosity and component, large specific surface area and diverse structure, MOF-based materials have been prepared and employed in diverse electrocatalytic fields, such as HER [33–36], oxygen evolution reaction (OER) [37–39], CO_2 reduction reaction [40–42] and NH_3 synthesis [43–45]. Furthermore, MOFs are ideal precursors to acquire functionalized MOFs derivatives like metal oxides, porous carbon or metal/carbon composites through pyrolysis, which represents an efficient strategy for the preparation of outstanding electrocatalytic materials [39,46,47]. Apart from the common merits with MOFs, MOF derivatives also demonstrate the following advantages: (1) MOF derivatives usually show enhanced stabilities compared with MOFs in electrocatalysis due to no break of coordination bonds or organic linkers; (2) Profiting from the formation of carbon after high-temperature pyrolysis, they show improved electrical conductivity; (3) Both metallic and non-metallic elements can participate in the formation of MOF derivatives, which may act as active sites for electrocatalysis. By virtue of the above advantages, various MOF-based materials have been developed as electrocatalysts in the past years [48–50]. To date, the EAS using MOF-based materials as electrocatalysts are still in the preliminary stage and few reviews have focused attention to summarize MOF based materials towards EAS [51]. Therefore, a timely summary and comprehensive review on the structure-activity relationship are conducive to develop superior MOF-based catalysts in the field of EAS.

In this review, we summarize recent progress of NH_3 synthesis from various nitrogen sources under ambient conditions over MOF-based electrocatalysts (Scheme 1). The mechanism of EAS via ERRs using various nitrogen sources as well as the quantification methods of ammonia are firstly analyzed and discussed in detail. Then we discuss the structural features and merits of MOF-based materials acted as electrocatalysts. Subsequently, recent advance in NH_3 synthesis from various nitrogen sources under ambient conditions over MOF-based electrocatalysts including pristine MOFs/MOF composites and MOF derivatives is summarized, and the effect of composition, structure and electronic properties of MOF-based electrocatalysts on the performance of EAS is analyzed and discussed. Finally, current challenges and future prospects of EAS are proposed. We believe that this review will provide the scientific guidance to explore the innovations of MOF-based materials for NH_3 synthesis.

2. Mechanism of EAS using various nitrogen sources and ammonia quantification

2.1. Mechanism of EAS using various nitrogen sources

For EAS, N_2, one of the main components of the atmosphere, is theoretically and experimentally studied as the feedstock by numerous researchers. In addition, the natural N cycle has been severely altered by the modern human activities, such as the excessive use of fertilizers and industrial production, which result in the deposition of undesired nitrogenous pollutants (NO_3^-/NO_2^-, gaseous NO_x, etc.) from the environment. Compared with the inert N_2, the nitrogenous pollutants are reactive N and can be thermodynamically easier to be reduced. Herein, we give an insight to the ERRs for EAS from various nitrogen sources.

2.1.1. N_2 reduction reaction (NRR)

Compared to the traditional H-B process, the electrocatalytic NRR to produce NH_3 under mild conditions can enable distributed NH_3 production using renewable electricity, reduce carbon emissions, ease the reactor design, and simplify the complexity of NH_3 production plants [17,52–54]. In the electrolytic cell, the NRR proceeds on the surface of cathode, which can be simply described as follows: N_2 molecules in the electrolyte are first adsorbed on electrode surface and then activated by the electrons supplied from external circuit along with stepwise hydrogenation to form NH_3. The half-reaction electrochemical NRR into NH_3 involves six electrons coupled protons transfer reactions and the corresponding equilibrium potentials versus reversible hydrogen electrode (vs. RHE) are as follows [52,55,56] :

Acidic media:

$$N_2(g) + 6H^+ + 6e^- \rightleftharpoons 2NH_3(aq) \quad E^{\ominus} = 0.092V \quad vs.RHE \tag{1}$$

Basic media:

$$N_2(g) + 6H_2O(l) + 6e^- \rightleftharpoons 2NH_3(aq) + 6OH^-(aq) E^{\ominus} = 0.092V \quad vs.RHE \tag{2}$$

From the point of the theoretical equilibrium potentials, the NRR can occur at room temperature and atmospheric pressure when an adequately negative potential is applied to an electrode [57]. Even so, the energy gap between the lowest unoccupied molecular orbital and the highest occupied molecular orbital of N_2 is up to 10.82 eV, indicating the great difficulty in the first-step activation of N_2 by electron, which corresponds to the much negative equilibrium potentials of 1 e^- reduction (Equation 3) [58,59]. What's more, the NRR into NH_3 is performed through multi-step proton-electron transfer reactions and multiple intermediates are involved (Equations 4–7), in which the redox potential for the formation of the N_2H intermediate is also much negative, suggesting the difficulty of the first H atom addition. Additionally,

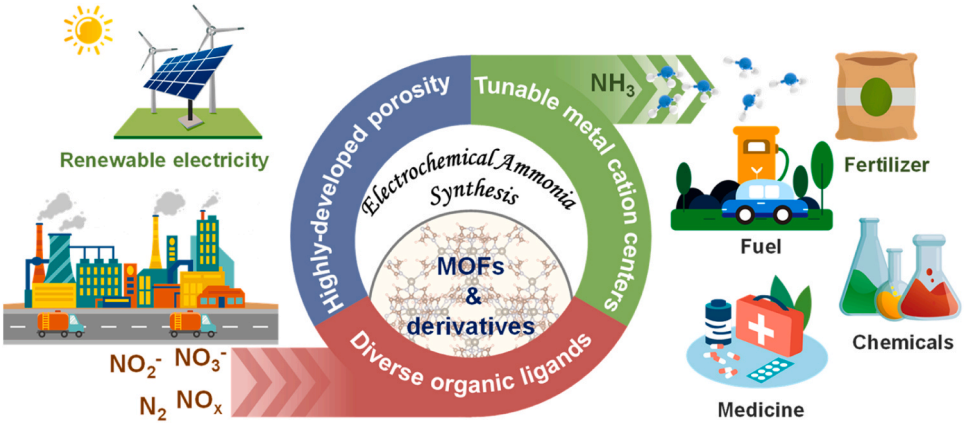

Scheme 1. Scheme of EAS from various nitrogen source.

considering the equilibrium potential of HER (0.00 V vs. RHE) is similar to that of NRR, the competition of HER in aqueous solutions is unavoidable. Thus, even though the EAS from NRR is thermodynamically favored, large barriers associated with the first activation and reduction processes to form favorable intermediate species and strong competition reaction of HER must be circumvented through effective catalyst design.

$$N_2(g) + e^- \rightleftharpoons N_2^-(aq) E^\ominus = -4.16V \quad vs.RHE \tag{3}$$

$$N_2(g) + H^+ + e^- \rightleftharpoons N_2H(g) E^\ominus = -3.2V \quad vs.RHE \tag{4}$$

$$N_2(g) + 2H^+ + 2e^- \rightleftharpoons N_2H_2(g) E^\ominus = -1.19V \quad vs.RHE \tag{5}$$

$$N_2H_2(g) + 2H^+ + 2e^- \rightleftharpoons N_2H_4(aq) \quad E^\ominus = 0.529V \quad vs.RHE \tag{6}$$

$$N_2H_4(aq) + 2H^+ + 2e^- \rightleftharpoons 2NH_3(aq) E^\ominus = 0.939V \quad vs.RHE \tag{7}$$

Electrolyte is an essential part for the electrochemical NRR to NH_3. In the past decades, various types of electrolytes including both solid and liquid electrolyte have been used in electrochemical cells for NH_3 synthesis, which are operated in a wide temperature range. According to the operating temperature, the electrochemical experiments studies can be classified as: high temperature (T > 500 °C), intermediate temperature (500 °C > T > 100 °C) and low temperature (T < 100 °C) [60]. In the high temperature range, solid-state proton (H^+) or oxygen-ion (O^{2-}) conductors, such as perovskites or materials with fluorite or pyrochlore structures, and suitable carbonates were developed as the electrolyte materials [61,62]. The mobile charge carriers in these electrolytes which ensure the circulation of the current circuit are usually H^+ or O^{2-} ion. And we can depict the reactor-cell design, electrode reactions and mobile charge carriers in these electrolytes as Fig. 1a, b. For the intermediate temperature range, molten salts (like chlorides, hydroxides), solid acids or the composite materials of solid oxides mixed with alkali metal salts were usually used as electrolyte [63–65]. Notably, in some reported alkali metal molten salts electrolytes, N_2 reacted with alkali metal and dissolved to nitride ions (N^{3-}), and the N^{3-} can also act as the charge carriers in the electrolysis process. The mobile N^{3-} in these electrolytes can be depicted as Fig. 1c. In the low temperature range, aqueous solutions, ionic liquids and polymer membranes were most commonly employed as the electrolytes, and H^+ ion or hydroxide (OH^-) ion usually acted as the charge carriers [66]. Fig. 1d shows a schematic diagram of NH_3 synthesis in the electrochemical cell using OH^- ion conducting electrolytes. Even though diverse electrolytes with different ion conductors have been explored for EAS via NRR, the conductivity of proton-conducting electrolytes in low temperature, such as Nafion, is much higher than of those of other ion conductors. Unfortunately, the reaction kinetics of NH_3 synthesis from N_2 are quite slow at low temperatures, which urgently need us to develop more efficient reactors and catalysts.

Apart from the direct hydrogenation of N_2 to NH_3, mediators (including lithium (Li), transition-metal compounds, metal-free complexes, and enzymes) have also been investigated as a bridge to not only circumvent the competitive HER but convert N_2 to NH_3 under ambient conditions. Among the mediator-strategies, the lithium-mediated high-efficiency electro-ammonia synthesis technology is expected to become an industrialized EAS technology due to metal Li can spontaneously react with nitrogen at room temperature and normal pressure. The proposed mechanism can be described as Equation 8 [67]:

$$3Li^+ + 1/2N_2 \xleftarrow{3e^-} Li_3N \xrightarrow{3BH} 3Li^+ + 3B^- + NH_3 \tag{8}$$

In the electrochemical synthesis process, Li metal first spontaneously reduces N_2 under ambient conditions to produce lithium nitride (Li_3N). Then, Li_3N reacts with a suitable proton carrier (BH) to generate ammonia and liberate Li^+ to restart the electrocatalytic cycle (Fig. 2) [24,68]. In 1993, Tsuneto et al. first carried out the electrochemical Li-mediated NH_3 synthesis using a single-compartment electrochemical cell equipped with a platinum anode and a metal cathode (Al, Ti, Mo, Fe, Co, Ni, Cu, Ag, Zn, and Pb) [69]. The electrolyte was tetrahydrofuran (THF) containing 0.2 M $LiClO_4$ and 0.18 M ethanol as proton source. In recent years, this idea has also been demonstrated experimentally by some researchers, and the current-to-NH_3 efficiency even closely approaching 100%. Nonetheless, the drawbacks that the high reduction potential required for electrochemical lithium cycle, lithium loss and safety issues related to handling the highly reactive metal Li exist and may block the application of the Li-mediated strategies at industrial scales, which need researchers overcome the technical barriers.

Recently, considering that direct conversion of N_2 to NH_3 either by H-B process or electrochemical NRR has practical drawbacks, two-step

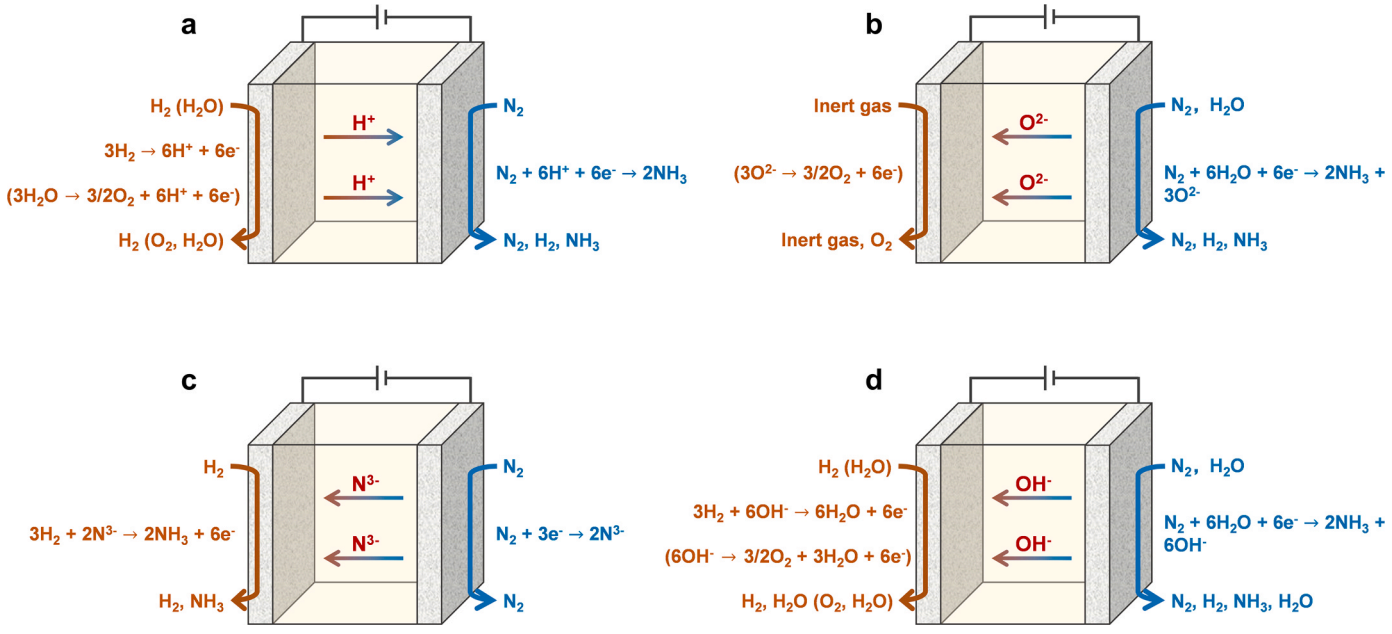

Fig. 1. Electrode reactions for NH_3 synthesis in electrochemical cells using (a) proton (H^+), (b) hydroxide ion (OH^-), (c) oxide ion (O^{2-}), and (d) nitride ion (N^{3-}) conducting electrolytes.
Reproduced with permission [56]. Copyright 2020 American Chemical Society.

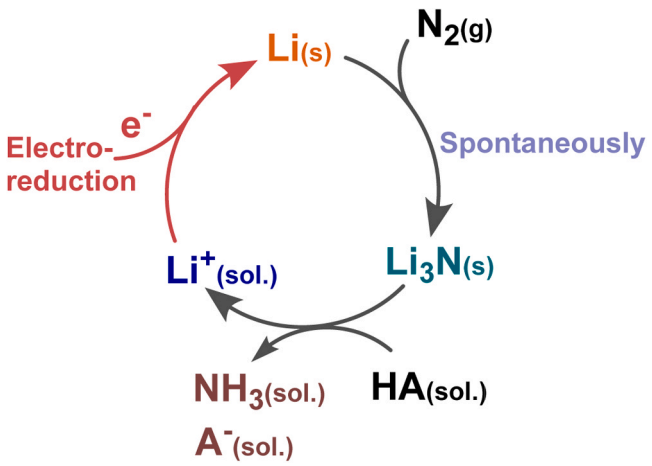

Fig. 2. The cycle of Li-mediated ammonia synthesis.
Reproduced with permission [24]. Copyright 2019 Elsevier.

process for NH_3 synthesis using N_2 as the feedstock has been explored. The innovative idea is that we can first convert the sluggish N_2 into more reactive species (such as nitrogen oxyanions) by eco-friendly and economical approach, which are then reduced to NH_3 through effective process. For example, Qiao et al. first employed the low-cost air and water as feedstocks for scale-up NH_3 synthesis under ambient conditions through two steps: (1) N_2 oxidization to NO_x^- by a facile plasma technique (pNOR) and (2) selectively electrocatalytic NO_x^- reduction (NO_x^-RR) to NH_3 (Fig. 3a) [70]. In the first plasma-driven N_2 oxidation step, the total NO_x^- yield can reach ca. 1.35 mmol h^{-1}. Then, the surface boron-rich core-shell nickel boride nanoparticle (Ni_3B@$NiB_{2.74}$) was developed as electrocatalyst to achieve ca. 100% conversion of as-obtained NO_x^- to NH_3. Additionally, Wu and co-workers demonstrated cobaloximes as a bioinspired molecular platform for EAS via electrocatalytic NO_x^-RR coupled with plasma-driven N_2 oxidation (Fig. 3b) [71]. Qiu's group used Cu nanoparticles (NPs) as a representative electrocatalyst to systematically investigated the plasma-enabled activation and recombination processes of N_2 and O_2 molecules as well as the mechanism of eNO_x^-RR at a microscopic level (Fig. 3c) [72]. The pNOR-eNO_x^-RR system is showed in Fig. 3d, in which N_2 and O_2 are first activated and converted into NOx species by the spark discharge, and then the NO_x^- ions are electrochemically reduced to NH_3 over Cu NPs. As shown in Fig. 3e, the concentrations of NO_2^-, NO_3^-, and NO_x^- gradually increase with the increase of spark discharge time. Accordingly, the NH_3 partial current density presents a rising tendency as the spark discharge time prolongating, suggesting the promotion effect of the spark discharge process on NH_3 synthesis (Fig. 3f). The strategy of "oxidation followed by reduction" provides new avenue and insight of renewable chemicals production by integrating various advanced technologies.

2.1.2. NO_3^-/NO_2^- reduction reaction (NO_3^-RR/NO_2^-RR)

Influenced by excessive anthropogenic activities, including the overuse of nitrogen-based fertilizers and the massive emission of industrial and domestic sewage, the amount of NO_3^- in surface water and underground is seriously excessive, threating the human health [73]. As discussed in Introduction, NO_3^- is easier to activate and absorb on the electrode surface than N_2, so that it is great meaningful and promising to use the green electricity to drive NO_3^- reduction reaction to value-added NH_3, which not only alleviates the environmental issues but also turns waste into wealth (Fig. 4) [74–77]. Considering the dissolved NH_4^+ can be easily collected using membrane separation technology or by heating distillation separation [78,79], the strategy of electrocatalytic NO_3^-RR for ammonia synthesis also can easily integrate with some mature industrial technologies, indicating its potential compatibility and flexibility towards scale up applications [80].

The reaction equation of electrochemical NO_3^-RR into NH_3 can be described as Equation 9, where SHE is the abbreviation of standard hydrogen electrode [81]:

$$NO_3^-(aq) + 9H^+(aq) + 8e^- \rightarrow NH_3(aq) + 3H_2O(g) E^{\ominus} = -0.12V \quad vs.SHE \tag{9}$$

While NO_3^-RR is a complicated and multi-step electron reduction and hydrogenation process, which involves the nitrogen-containing intermediate species from + 5 to − 3 valence states. As for the electrocatalytic mechanism, two pathways have been proposed by M.T.M. Koper: indirect reduction and direct reduction [82]. The indirect reduction of NO_3^- is an autocatalytic procedure, in which NO_3^- itself does not participate in the electron-transfer process but other intermediate species can be involved in the electron transfer reaction. The indirect reduction mechanism is experimentally verified only in the highly acidic environments (> 1.0 M) with high NO_3^- concentration (> 1.0 M) and at low overpotentials (0.8–0.9 V vs. SHE). The direct electroreduction of nitrate can be described as follows: (1) NO_3^- is stepwise reduced by the adsorbed active hydrogen atom (H_{ads}*), which is generated from H_2O reduction by electron on the cathode surface, and the intermediates species may be NO_{2ads}^-, NO_{ads}, N_{ads}, NH_{ads}, NH_{2ads}, and so on; (2) NO_3^- reacts with the electrons on cathode surface and is simultaneously hydrogenated by H^+ in the electrolyte (Fig. 5) [81]. When the NO_3^- is at low concentrations (below 0.1 M), the direct reduction mechanism may mainly execute. During the electron/H^+ reduction mechanism, the reduction of NO_3^- to NO_2^- is the rate-determining step and the reaction rate is directly affected by the adsorption capacity of NO_3^- on the electrocatalysts surface. Additionally, NO_{ads} is the divergent center towards N_2O, N_2, and NH_3 product, suggesting the subsequent electroreduction pathway of NO_{ads} determine the selectivity of NO_3^-RR to NH_3 [83]. Thus, the ideal electrocatalyst should not only better adsorb and activate NO_3^- but also functionally electro-reduce NO_{ads} to NH_3.

Apart from NO_3^-, NO_2^- is the most common N-contaminant in the aquatic ecosystem, which threats to the survival of organisms. In recent years, researchers also have employed NO_2^- as the nitrogen source for EAS [71,85–87]. Similarly, electrocatalytic NO_2^-RR involves complex six electrons transfer and multi-step hydrogenation process described as Equation 10 (Fig. 6) [84].

$$NO_2^-(aq) + 8H^+(aq) + 6e^- \rightarrow NH_4^+(aq) + 2H_2O(l) \tag{10}$$

Thus, the challenge that controlling the selectivity of desired product urges researchers to develop effective reaction systems with high efficiency and specificity for electrochemical NO_2^-RR.

2.1.3. Gaseous NO_x reduction reaction (NO_xRR)

Gaseous NO_x (NO and NO_2, etc.) are important air pollutants that can cause severe environmental issues, such as acid rain, photochemical smog, and so on [88]. It is estimated that about 53 million tons of nitrogen oxides are emitted in the atmosphere by human activities (industrial production, motor vehicle exhaust, etc.) worldwide every year. Currently, the mature strategies for the reduction of NO_x can be summarized as two kinds: reducing NO_x emission by optimizing the general combustion process and selective catalytic reduction of NO_x into non-toxic N_2 [89]. Both the two methods are less economical than recently proposed strategy that NO_x reduction to NH_3 using the renewable energy, which not only eliminates the toxic NO_x contaminant in the air but also synthesizes high value-added NH_3 (Fig. 7) [90]. Since nitric oxide (NO) is the only insoluble nitrogen oxide, researchers pay more attention to designing efficient electrocatalysts for NO reduction to NH_3. The total reaction formula of electrocatalytic NO reduction reaction (NORR) to NH_3 can be described as Equation 11 [91]:

$$NO(g) + 6H^+(aq) + 5e^- \rightarrow NH_4^+(aq) + H_2O(l) \tag{11}$$

For the reaction mechanism of NORR, two main pathways were proposed: (1) NO → NO* → NOH* →HNOH* → NH* → NH_2 * → NH_3

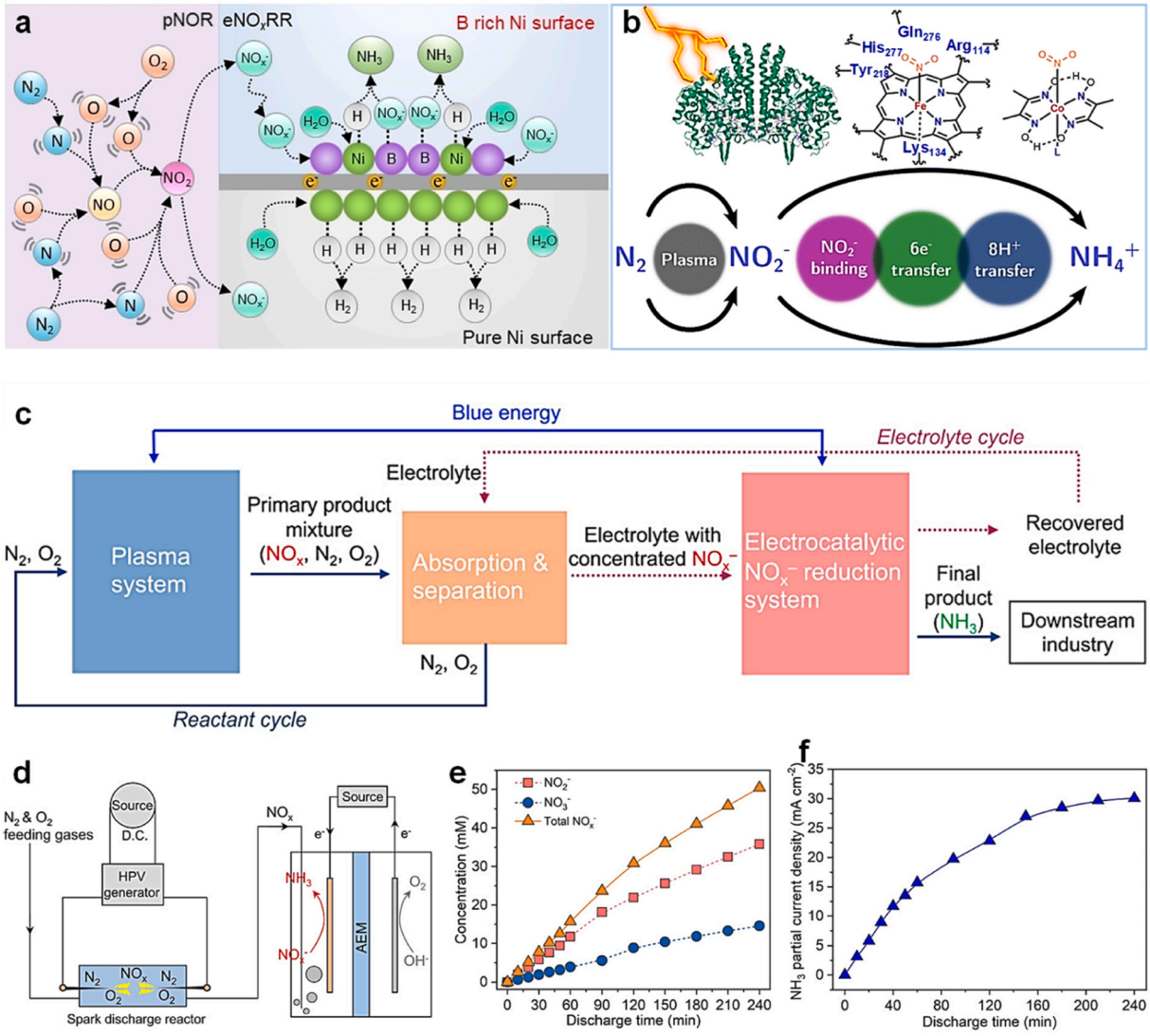

Fig. 3. (a) The pNOR + eNO$_x$RR process and dual-site mechanism for boosted eNO$_x$RR activity, (b) NH_3 synthesis via NO_2^- by natural cytochrome *c* nitrite reductase and cobaloxime electrocatalysts. (c) Illustration for the proposed pNOR-eNO$_x^-$RR process integration system. (d) Illustration for the plasma-enabled cascade pNOR-eNO$_x^-$RR integrated system, (e) Concentrations of NO_2^-, NO_3^-, and total NO_x^- as the function of spark discharge time, (f) NH_3 partial current density as a function of spark discharge time in the range of 0–240 min.
Reproduced with permission [70]. Copyright 2021, Wiley-VCH. Reproduced with permission [71]. Copyright 2022, Royal Society of Chemistry. Reproduced with permission [72]. Copyright 2022, American Chemical Society.

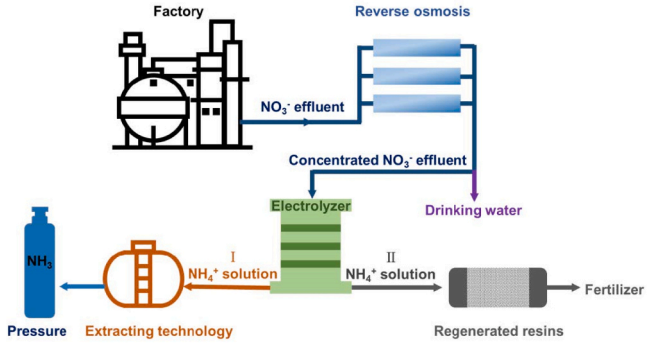

Fig. 4. The schematic illustration for incorporating nitrate-to-ammonia technique into present technological processes.
Reproduced with permission [80]. Copyright 2020, Wiley-VCH.

* → NH_4^+ and (2) NO → NO* → NOH* → N * →NH* → NH_2 * → NH_3 * → NH_4^+, both where the adsorbed NOH* is the pivotal intermediate [90,92].

2.2. Methods of ammonia quantification

The accurate detection and quantification of NH_3 are crucial for evaluating the performance of EAS. So far, several analysis methods are commonly used including colorimetric method, ion chromatography (IC) method, ammonia ion-selective electrode and ^{1}H NMR spectroscopy method, and the assess of partial common techniques can be seen in Fig. 8 [93]. Some other methods, such as fluorometric method [94,95], conductivity method [96], titrimetric method [97], and enzymatic method [98], can also quantify the dissolved NH_3 concentration but less used in the electrochemical ammonia field.

Colorimetric method is the most common detection method used in the laboratory due to the low cost and its high precision, mainly including three categories: Nessler's reagent method, indophenol blue method and salicylate method. Firstly, the Nessler's reagent, developed

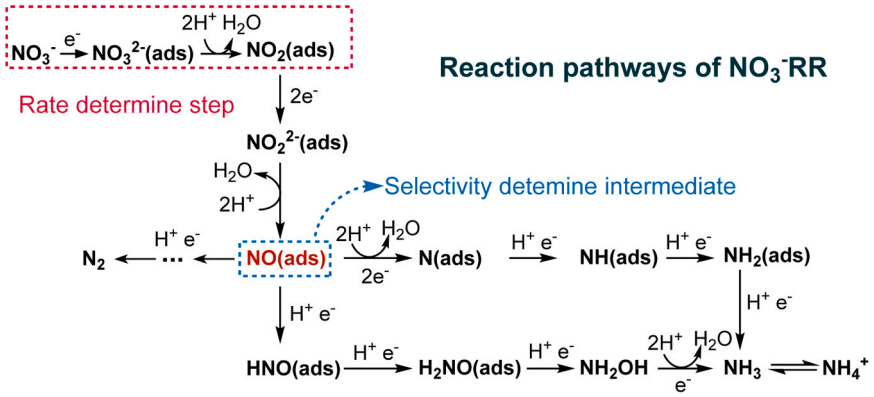

Fig. 5. Schematic illustration of reaction pathways for NO_3^- reduction over electrocatalysts.
Reproduced with permission [81]. Copyright 2021, Royal Society of Chemistry.

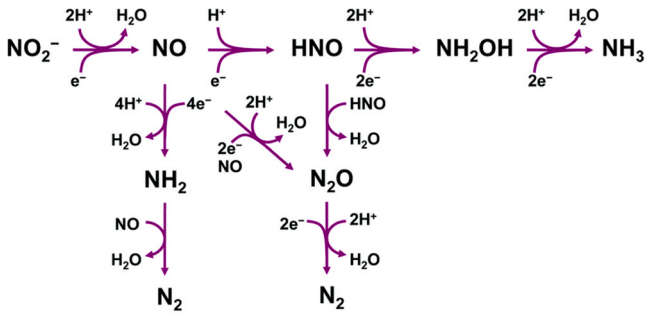

Fig. 6. The pathway of electrochemical NO_2^-RR to different products.
Reproduced with permission [84]. Copyright 2022, Royal Society of Chemistry.

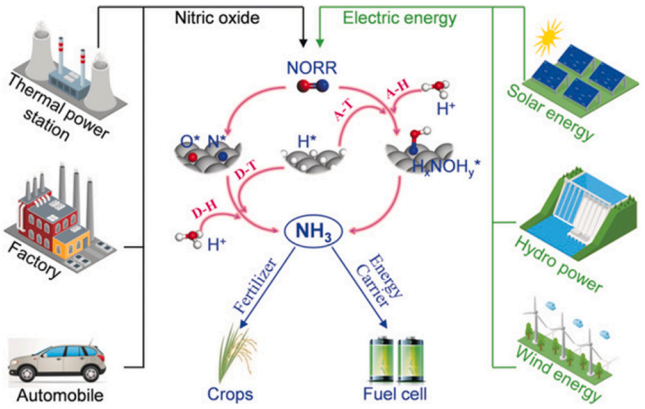

Fig. 7. Illustration of the proposed EAS route from NO.
Reproduced with permission [90]. Copyright 2020, Wiley-VCH.

by Julius Nessler in 1856, consists of mercury (II) iodide (HgI_2) and potassium iodide (KI), which react to form potassium tetraiodomercurate (II) (K_2HgI_4), in an alkaline solution (KOH or NaOH) [99]. When added to the low-concentration NH_3 solution, Nessler's reagent reacts with NH_3 to form a colored colloidal solution, which can be detected through UV-spectroscopy at wavelength of 420 nm. The detection limit of this method can reach to be 0.02 ppm. It is noteworthy that Nessler's reagent method for ammonia detection is easily interfered by some metal cations (Fe^{3+}, Mn^{2+}, Mg^{2+}, etc.), hydrazine, carbonyl compounds, etc. Usually, potassium sodium tartrate tetrahydrate, $KNaC_4H_4O_6{\cdot}4H_2O$) solution is added before Nessler's reagent to eliminate the interference of cations. Then, the indophenol blue method, which can detect the NH_3 at low concentration of 0.02–1.25 ppm, is based on the Berthelot reaction [100]. In this method, blue colored indophenol is formed after the reaction of NH_3 with hypochlorite and phenol in the alkaline medium, which can be detected through UV-spectroscopy at wavelength range of 630–650 nm. In this reaction system, sodium nitroprusside ($Na_2[Fe(CN)_5NO]_5$) is added as catalyst to accelerate the reaction and citrate is also used to prevent the ion precipitation which could be produced in the alkaline condition. The indophenol blue method is sensitive to NH_3 but is not suitable for detection of high concentrations of NH_3 because excess NH_3 could suppress the indophenol blue reaction [101]. Additionally, it is slightly interfered by the organic nitrogen compounds, nitrite, nitrate, Ca^{2+}, Mg^{2+} and various electrolytes [102–105]. To avoid using the noxious phenol and producing toxic volatiles during the detection employing indophenol blue method, the salicylate method is developed by replacing phenol with salicylate [106,107]. The color development mechanisms of the two methods are similar but the salicylate method is much safer. Quantitative measurements are usually performed through UV-spectroscopy at the wavelength of 640 nm.

Compared with the colorimetric methods, the IC method is more convenient and efficient for ammonia (especially low-concentration ammonia) detection due to its high sensitivity (detection limit of 3×10^{-7} mol L^{-1}), good reproducibility, high stability and pH compatibility [108,109]. In the instrument, the cations are separated through the columns filled with cation-exchange materials and identified by those characteristic retention times individually. And the quantitative analysis of ammonia is based on the comparison of the obtained peak areas with those of standard samples. Note that, the ions with very close retention times like Li^+ and Na^+ could interfere with each other due to the overlap or overlay of peaks [110]. To improve the reliability and accuracy of

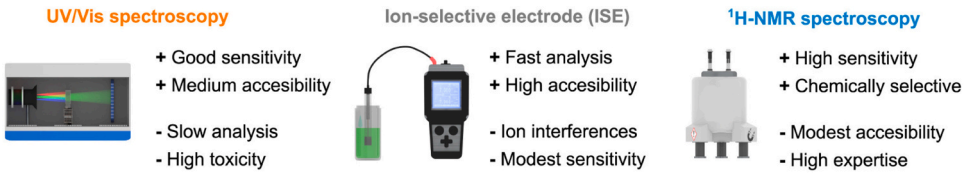

Fig. 8. Ammonia quantification techniques assessed with pros (+) and cons (−).
Reproduced with permission [93]. Copyright 2020, Elsevier.

ammonia quantification in practical EAS experiments, Yang and co-workers evaluated the accuracy and precision of IC by taking the pH values of electrolyte, the interference Li^+, Na^+, 14 kinds of common transition-metal cations (5000 mg L^{-1}) and 5 kinds of common organic compounds, background and reagents into consideration [111]. According to the analysis results, a rigorous test process is recommended and showed in Fig. 9 to accurately quantify NH_4^+ by IC method.

The ISE method is sensitive for NH_3 detection which can show a much larger detection range (0.03–1400 mg L^{-1}) [112]. It contains an ammonia ion-sensitive electrode which has a poly(vinylchloride) (PVC) membrane, a reference electrode and voltmeter. Based on the Nernst equation, the potential difference between PVC membrane and the reference electrode depends on the concentration of free ammonium ions in the solution. So, before the measurement, the dissolved ammonia must be completely converted to ammonia ions by adjusting the pH of the tested solution. And, the concentration of ammonium ions in the sample solution is quantified by the standard curve gained from known concentrations of ammonium ions. In the method, some common cations (especially K^+) with high concentrations may affect the measurement accuracy.

Another commonly used quantified method of ammonia is ^1H NMR spectroscopy which generally combined with $^{15}N_2$ isotopic labeling experiments [80,113,114]. The $^{15}N_2$ isotopic labeling experiments by replacing $^{14}N_2$ with $^{15}N_2$ as the feedstock is also employed to verify the origin of the produced NH_3. To quantified ammonia concentration, internal standard and external standard methods are generally used. In the internal standard method, maleic acid ($C_4H_4O_4$) with definite concentration is used as the internal standard due to it contains only one chemical shift of H ($\delta \approx 6.29$ ppm) and does not interfere the signal peaks of ammonia. And the quantitative analysis of ammonia is based on the comparison of the obtained peak areas with those of maleic acid. As for external standard methods, a series of ammonia solutions with known concentrations are tested and the standard curve related to the peaks area and concentration is then drew to quantify the sample solution.

Although each of mentioned methods can be able to accurately detect the concentration of ammonia under certain conditions, combining two or more methods is proposed to more reliably and convincingly quantify the ammonia [109,115].

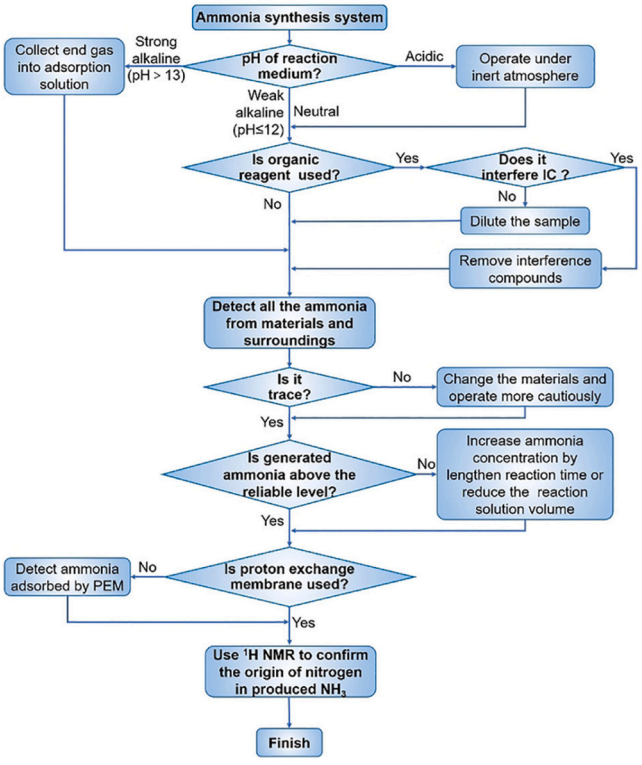

Fig. 9. Flowchart of recommendations that should be considered when performing ammonia synthesis experiments and detecting NH_4^+ by IC method. Reproduced with permission [111]. Copyright 2019, Wiley-VCH.

3. Structural features and merits of MOF-based electrocatalysts

MOFs are a novel kind of organic-inorganic hybrid crystalline materials with highly ordered porous structure, in which metal cation centers are coordinated with organic ligands to form three-dimensional frameworks [116,117]. To date, more than 20,000 different MOFs have been reported and studied, and it is foreseeable that novel MOFs will continue to be developed in the future [118,119]. Recently, MOF-based materials as electrocatalysts have exhibited distinctive performance because of their unique structural features and merits. Notably, MOFs, usually composed of metal ions and redox-inactive organic ligands, lack free charge carriers and charge transport paths, which show electrical insulator property, resulting in low utilization of active sites of MOFs [120]. To improve the electrical conductivity of pristine MOFs, constructing freestanding MOFs on conductive substrates and intrinsically conductive MOFs, and combining MOFs with conductive materials like nanostructured carbon materials or metal, and conductive polymers to form MOF composites are commonly used methods [120–123]. Additionally, MOFs can be used as templates or precursors to obtain MOF-derived materials (e.g., carbon materials, metal oxides, metal oxides/carbon composites) through thermal treatment, which usually show improved electrical conductivity [119,124–127]. Herein, based on above considerations, we demonstrate structural features and merits of MOF-based electrocatalysts using the classification of pristine MOFs/-MOF composites and MOF derivatives as follows.

3.1. Pristine MOFs/MOF composites

In pristine MOFs/MOF composites, the metal centers generally refer to the metal ions or metal clusters with unoccupied orbitals, and the multidentate organic ligands which contain nitrogen, oxygen, sulfur and so on [128,129]. Benefiting from the diversity of coordination, MOFs/MOF composites own the inherent advantages of highly-developed porosity, tunable composition and structure, so that they have been widely applied in gas adsorption and separation, catalysis, fluorescent sensing and so on [130–134]. The merits and uniqueness of MOFs/MOF composites as the catalytic materials for electrochemical energy conversion can be mainly summarized into the following three aspects:

(1) Highly-developed porosity.

Most prominent feature of MOFs is the highly porous structures, which can provide a large area of active interface and evenly dispersed active sites for catalytic reactions. When the MOFs are used as supporting substrate, the abundant pores suggest more hosted sites for active materials and the crystalline frameworks can also further ensure the uniform distribution and efficient immobilization of active materials [135]. In addition to the large active area, the ordered pores show spatial confinement of reactants and provide smooth mass transport channels for the diffusion of electrolyte, which promotes the delivery of reactants and the desorption of products towards and from catalytic sites, thus ensuring the continuous proceedings of the catalytic reaction [136,137]. More attractively, unlike other types of porous materials, the porosity of MOF materials can be predicted or designed through the selection of the metal cations and ligands with specific coordination geometry and connectivity [138].

(2) Tunable metal cation centers.

As the core component, metal cations play a central role in determining the structures and functionalities of MOFs [139,140]. The type and amounts of unoccupied orbitals in metal cation influences the

spatial arrangement of the coordinated ligands and thus determines the pore shape and size of the porous framework. In this respect, preconceived MOFs with specific structure and function can be designed through tuning the metal cation centers. Thanks to the ordered arrangement of metal cations and ligands in MOFs, metal cations are atomically distributed in the framework, which maximizes the utilization of metallic active sites. In addition, when the types and amounts of unoccupied orbitals of two or more metal cations are analogous, multi-metallic centers can be incorporated in the framework and the metal cations are orderly arranged. For the ordered multi-metallic centers, synergistic effects or/and electron interaction may exist in the different active sites, thus improving the catalytic performance. Moreover, the multi-metallic cations can also take effect on the structural modulation. Taking the bimetallic MOF materials as examples, when one of the bimetallic cations acts as the active site, the other can take part in modulating the porous structure.

(3) Diverse organic ligands.

Organic ligands are the linkers for the distributed metal cations centers through the coordination, which play the role of "skeleton" in MOFs [141]. So diverse selection and design of organic ligands can greatly affect the properties and functions of MOFs. Additionally, organic ligands can also be the source of other non-metallic elements, such as nitrogen, phosphorus and sulfur, which can modify the electronic property of active metal center or directly one-step react with metal cations, partially transition metals, into metal compounds in the MOF derived carton materials [142].

3.2. MOF derivatives

Thanks to their characteristic merits, pristine MOFs or their composites have been under intensive studies in electrocatalytic fields. However, they generally face the issues of low stability and electrical conductivity, which greatly hinder the practical application. In this case, by controlled conversion processes like thermal or chemical treatments, MOFs can be converted into their derivatives, including single-metal site catalysts, heteroatom-doped carbon, metal or metal oxide clusters/particles and their complexes, etc., which have a good prospect in the field of electrocatalytic energy conversion [39,143–146]. Based on the unique advantages of MOFs precursors, MOF derivatives can also inherit the structural features and merits such as controllable hierarchical porous structures with rich and highly dispersed active sites and tunable chemical compositions [147]. Additionally, MOFs can easily be incorporated with various external components such as organic molecules, metal nanoparticles, polyoxometalates and polymers, which can serve as functional components or regulators that induce the formation of targeted and functionalized derivatives [148]. More importantly, MOF derivatives usually show improved electrical conductivity benefited from the carbon formation and enhanced stability for electrocatalysis because no breaks of coordination bonds occur in the derivatives [149]. And both metallic and non-metallic elements can participate in the formation of MOF derivatives, which may act as active sites for electrocatalysis [150]. Lastly, the low-cost and simple synthesis process offers potential large-scale production routes of MOF derivatives for eventual industrial applications.

4. MOF-based electrocatalysts for EAS from various nitrogen sources

Based on above discussions, using the classification of MOF-based electrocatalysts including pristine MOFs/MOF composites and MOF derivatives, we summarize recent progress of NH_3 synthesis via ERRs from various nitrogen sources under ambient conditions in this section. More intuitively, the advanced pristine MOFs/MOF composites and MOF derivatives as electrocatalysts for EAS from various nitrogen sources are listed in Table 1 and Table 2, respectively.

4.1. Pristine MOFs/MOF Composites

4.1.1. NRR

Tunable chemical environments of the pores or channels and periodical arranged metal sites of MOFs make they have great potential to concentrate and activate N_2, thus they have attracted great interest to serve as electrocatalysts for ammonia synthesis from N_2 reduction [45,174,175]. In 2017, Zhao and co-workers first reported the application of

Table 1
Summary of pristine MOFs/MOF composites as electrocatalysts for EAS from various nitrogen sources.

Nsource	Catalyst	Electrolyte	NH_3 Yield	FE	Detection method	Ref.
N_2	PCN-222(Fe)	0.1 M HCl	110.9 μg h^{-1} mg_{cat}^{-1}	70.7%	Nessler's reagent	[45]
	In-MOF	0.05 M $H_2SO_4$0.01 M KOH	24.70 μg h^{-1} mg^{-1}79.20 μg h^{-1} mg^{-1}	6.72% 14.98%	Indophenol blue	[151]
	NiFe-MOF	0.1 M $NaHCO_3$	9.3 μg h^{-1} mg_{cat}^{-1}	11.5%	Indophenol blue	[152]
	HT Au@MOF	0.1 M Na_2SO_4	49.5 μg h^{-1} mg_{cat}^{-1}	60.9%	Nessler's reagent	[153]
	60 nm Pt/Au@ZIF	$LiCF_3SO_3$ (0.2 M) in ethanol (1%)/THF	161 μg mg_{cat}^{-1} h^{-1}	44%	Indophenol blue	[154]
	Ag-Au@ZIF	$LiCF_3SO_3$ (0.2 M) in ethanol (1%)/THF	10pmol cm^{-2} s^{-1}	18%	Indophenol blue	[155]
	ZIF-67 @Ti_3C_2	0.1 M KOH	6.52μmol h^{-1} cm^{-2}	20.2%	Indophenol blue	[156]
	MoS_2 @ZIF-71	Na_2SO_4	56.69 μg h^{-1} mg_{cat}^{-1}	30.91%	Indophenol blue	[157]
	NCNT@MIL-101(Fe)	0.05 M H_2SO_4	6.97 μg h^{-1} mg_{cat}^{-1}	25.15%	Indophenol blue	[158]
	MIL-101(Fe)/MoS_3	0.1 M HCl	25.7 μg h^{-1} mg_{cat}^{-1}	36.71%	Indophenol blue	[159]
	PdCu@UiO-S@PDMS	0.1 M HCl	20.24 μg h^{-1} mg_{cat}^{-1}	13.16%	Indophenol blue	[160]
	Co_3Fe-MOF	0.1 M KOH	8.79 μg h^{-1} mg_{cat}^{-1}	25.64%	IC	[161]
	UiO-66-NH_2	0.1 M Na_2SO_4	52.81 μg h^{-1} mg_{cat}^{-1}	85.21%	Indophenol blue	[162]
	Pd-TA	0.1 M Na_2SO_4	24.12 μg h^{-1} cm^{-2}	9.49%	Indophenol blue	[163]
	NPG@ZIF-8	0.1 M Na_2SO_4	28.7 μg h^{-1} cm^{-2}	44%	Indophenol blue	[54]
	Fe-TCPP	0.1 M HCl	44.77 μg h^{-1} mg_{cat}^{-1}	16.23%	Indophenol blue	[164]
	Cu@Ce-MOF	0.1 M KOH	14.83 μg h^{-1} cm^{-2}	10.81%	Indophenol blue	[165]
	MIL-100 (Al)	0.1 M KOH	10.6 μg h^{-1} cm^{-2} mg_{cat}^{-1}	22.6%	Indophenol blue	[166]
NO_3^-/ NO_2^-	Cu@CuHHTP	0.5 M Na_2SO_4 + 500 ppm NO_3^-	1.84 mg h^{-1} cm^{-2}	67.55%	Indophenol blue	[167]
	NiCoBDC@HsGDY	1.0 M KOH + 0.1 M NO_3^-0.5 M Na_2SO_4 + 0.1 M NO_3^-	0.56 mmol h^{-1} cm^{-2}0.39 mmol h^{-1} cm^{-2}	99.1%99.7%	Nessler's reagent	[168]
	$Cu_3(BTC)_2$ @HsGDY	0.5 M Na_2SO_4 + 200 ppm KNO_3	0.24 mmol h^{-1} cm^{-2}	90.2%	Nessler's reagent	[169]
	Pd-NDs/Zr-MOF	0.1 M Na_2SO_4 + 500 ppm NO_3^-	287.31 mmol h^{-1} g_{cat}^{-1}	58.1%	Indophenol blue	[170]
	Ru_xO_y/RuNi-MOF	0.1 M Na_2SO_4 + 50 ppm NO_3^--N	274 μg h^{-1} mg_{cat}^{-1}	72.56%	Nessler reagent	[171]
	Fe_2Co-MOF	0.05 M H_2SO_4 + 50 g L^{-1} KNO_3	3463.3 μg h^{-1} mg_{cat}^{-1}	90.55%	Indophenol blue	[172]
	UiO-CuZn	0.5 M Na_2SO_4 + 200 ppm NO_3^-	0.22805 mmol g^{-1} h^{-1}	91.4%	Indophenol blue	[173]

Table 2
Summary of MOF derivatives as electrocatalysts for EAS from various nitrogen sources.

N source	Catalyst	Electrolyte	NH_3 Yield	FE	Detection method	Ref.
N_2	S/N-MPC	0.05 M H_2SO_4	45.51 μg_{NH3} mg_{cat}^{-1} h^{-1}	25.16%	Indophenol blue	[185]
	Co@NC	0.1 M Na_2SO_4	1.58 × 10^{-10} mol s^{-1} cm^{-2}	21.79%	Indophenol blue	[186]
	NC@Ru-5	0.1 M KOH	16.68 μg h^{-1} mg_{cat}^{-1}	14.23%	Nessler's reagent	[187]
	Fe_2O_3 @ -MoS_2	0.1 M Na_2SO_4	112.15 μg h^{-1} mg_{cat}^{-1}	8.62%	Indophenol blue	[188]
	CoRu@NC	0.1 M KOH	56.82 μg h^{-1} mg_{cat}^{-1}	2.02%	Nessler's reagent	[189]
	TiO_2/CeO_2	0.1 M HCl	8.8 μg h^{-1} mg_{cat}^{-1}	22.3%	Indophenol blue	[190]
	Ru SAs/N-C	0.05 M H_2SO_4	120.9 μg_{NH3} mg_{cat}^{-1} h^{-1}	29.6%	Indophenol blue	[191]
	Fe_1-N-C	0.1 M HCl	1.56 × 10^{-11} mol cm^{-2} s^{-1}	4.51%	Indophenol blue	[192]
	Mo-SA/PNC	0.05 M H_2SO_4	15.34 μg h^{-1} mg^{-1}	24.03%	Indophenol blue	[180]
	MoFe-PC	0.1 M HCl	34.23 μg h^{-1} mg_{cat}^{-1}	16.83%	Indophenol blue	[193]
	Mo-Co/NC	0.1 M Na_2SO_4	89.8 μg h^{-1} mg_{cat}^{-1}	13.5%	Indophenol blue	[194]
	C-Ti_xO_y/C	0.1 M $LiClO_4$	14.8 μg h^{-1} mg_{cat}^{-1}	17.8%	Indophenol blue	[195]
	CoP HNC	1.0 M KOH	10.78 μg h^{-1} mg_{cat}^{-1}	7.36%	Indophenol blue	[196]
	C@YSZ	0.1 M Na_2SO_4	24.6 μg h^{-1} mg_{cat}^{-1}	8.2%	Nessler's reagent	[197]
	ISAS-Fe/NC	0.1 M PBS	62.9 μg h^{-1} mg_{cat}^{-1}	18.6%	Indophenol blue	[198]
	MoP@PPC	0.1 M HCl	28.73 μg h^{-1} mg_{cat}^{-1}	2.48%	Indophenol blue	[199]
NO_3^-/ NO_2^-	Co@NC	0.1 M NaOH+ 0.1 M NO_3^-	758μmol h^{-1} mg_{cat}^{-1}	96.5%	Indophenol blue	[200]
	Cu@C	1.0 M KOH+ 1 mM NO_3^-	469.5 μg h^{-1} cm^{-2}	72%	Indophenol blue	[201]
	Cu(I)-N_3C_1 SAC	50 mM Na_2SO_4 + 100 ppm NO_3^--N	50.3μmol mg_{cat}^{-1} h^{-1}	65.3%	Nessler's reagent	[202]
	Cu/Pd/CuOx	0.5 M K_2SO_4 + 50 mg L^{-1} NO_3^--N	1510 μg h^{-1} mg_{cat}^{-1}	84.04%	Nessler's reagent	[203]
	$Ru_{15}Co_{85}$	0.1 M KOH+ 0.1 M KNO_3	3.21 mol g_{cat}^{-1} h^{-1}	96.78%	salicylate ^{1}H NMR	[204]
	CuNi/NC	0.1 M PBS+ 50 mg L^{-1} NO_3^--N	n/a	79.6%	Gas-phase molecular absorption spectrograph	[205]
	Ru SA-NC	1.0 M KOH+ 0.5 M NO_3^-1.0 M KOH+ 0.5 M NO_2^-	0.11 mmol h^{-1} cm^{-2}0.69 mmol h^{-1} cm^{-2}	72.8% 97.8%	Indophenol blue	[206]
	Cu-N-C	1.0 M KOH+ 1.0 M KNO_3	13.8 mol_{NH3} g_{cat}^{-1} h^{-1}	95.5%	Nessler's reagent	[207]
	Cu/Ni-NC	0. 5 M Na_2SO_4 + 100 ppm NO_3^--N	5480 mg h^{-1} mg_{cat}^{-1} cm^{-2}	97.28%	Nessler's reagent	[208]
	MR Co-NC	0.1 M KOH+ 0.1 M KNO_3	1.25 mmol h^{-1} cm^{-2}	95.35%	IC	[209]
NO	Co-NPs	0.1 M PBS+NO	244μmol mg_{cat}^{-1} h^{-1}	92.3%	H NMR	[210]

MOFs as NRR electrocatalysts at low temperature and ambient pressure [176]. A series of MOFs (M) (M = Fe, Co, Cu) were synthesized in this work, among which the Fe-based MOF displayed the best catalytic activity: NH_3 yield and a low faradaic efficiency (FE) value are 2.12 × 10^{-9} mol s^{-1} cm^{-2} and 1.43%, respectively, at 1.2 V and 90 °C using pure N_2 and water as raw materials. According to their results, porous MOFs can offer massive metal sites with empty D-orbitals, which served as N_2 adsorbent and Lewis acid to adsorb and activate N_2 molecules on the electrode surface. Afterwards, more monometallic MOFs, such as Fe, Co, Zn, Cu, Al, Zr, Ce, and In, have been explored for NH_3 synthesis via NRR. Typically, Zhang et al. developed well-defined single-site MOFs (M-TCPP; M = Fe, Co, or Zn) as electrocatalysts for electrocatalytic N_2 reduction. The prepared Fe–TCPP showed outstanding performance with high NH_3 yield of 44.77 μg h^{-1} $mg_{cat.}^{-1}$ and FE of 16.23%, superior to

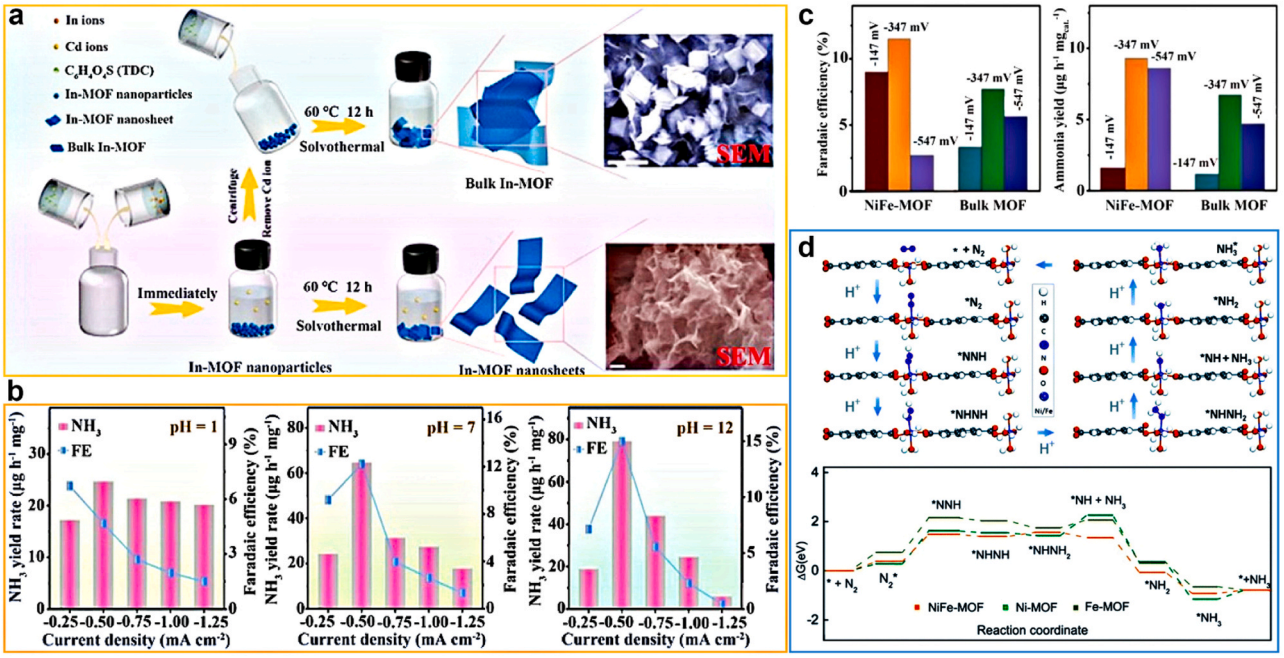

Fig. 10. (a) The synthesis and morphological characterization of In-MOF nanosheets. (b) NRR performances of In-MOFs in different pH electrolytes. (c) FEs and NH_3 yields of NiFe-MOF and bulk MOF at different potentials, (d) Density functional theory calculations of NiFe-MOF and its counterparts
Reproduced with permission [151]. Copyright 2021, Royal Society of Chemistry. Reproduced with permission [152]. Copyright 2020, Royal Society of Chemistry.

those of most reported MOF catalysts. This work expounded the single Fe site promoted the formation of the key *NNH intermediate during the hydrogenation of N_2. Although pristine MOF materials as NRR electrocatalysts show potential applications, the poor conductivity is a tough obstacle in electrocatalytic applications. In this regard, conductive two-dimensional (2D) MOF nanosheets are considered more attractive candidates based on some theoretical predicts [177,178]. Duan and co-authors prepared 2D In-MOFs nanosheets with a thickness of 1.3 nm via an ion exchange and dissolution-recrystallization mechanism (Fig. 10a) [151]. Benefited from the high porosity and excellent electrical conductivity, the 2D In-MOFs exhibited excellent electrocatalytic NRR performance in a full pH range: The maximum NH_3 yields of 24.70, 64.73, and 79.20 μg h^{-1} mg^{-1} at different the pH value of 1, 7, and 12, respectively (Fig. 10b). Except for the improvement of the conductivity, incorporating second or third metal ions into the MOF materials is a good strategy to adjusting the center value of D-band of metals to enhance their catalytic performance. For example, Zhao group reported bimetallic NiFe-MOF NPs with an average particle size of 5.5 ± 1.8 nm as electrocatalyst for NRR. The NiFe-MOF nanodots showed the excellent catalytic activity of NH_3 yield (9.3 μg h^{-1} $mg_{cat.}^{-1}$) and FE (11.5%) at − 0.374 V versus RHE at ambient temperature (Fig. 10c) [152]. Mechanistic investigations reveal that the better NRR activity of bimetallic MOFs than that of the corresponding monometallic materials is attributed to the synergy of both Fe and Ni cations in the bimetallic system. And theoretical research highlights the iron doping effect can suppress the energy barrier of the first ammonia release step (Fig. 10d).

Based on the rich well-defined porosity, MOFs possess large surface areas, which can also be implemented as host for high-active metal nanoparticles. The active metal nanoparticles are confined in the channels, which can effectively inhibit the aggregation of the particles during the catalytic process. Meanwhile, the hydrophobicity of MOF matrixes can efficiently suppress the mass transfer of H_2O and further weaken the competitive HER during the aqueous electrocatalytic N_2 reduction. For example, Du and co-authors developed a porous three-dimensional (3D) Zn-based MOF with high porosity and rich disulfide bonds to confine Au NPs with ultrafine size of 1.9 ± 0.4 nm through integration of dynamic covalent chemistry and coordination chemistry [153]. Subsequently, Au@MOF was modified with organosilicon to enhance the hydrophobicity, which can strongly inhibit the competitive HER (Fig. 11a). The active Au particles were confined in the caged-shaped Zn-based MOFs (Fig. 11b, c). Consequently, the hydrophobic Au@MOF composite shows excellent electrocatalytic NRR performances: the highest NH_3 yield of 49.5 μg h^{-1} $mg_{cat.}^{-1}$ and FE of 60.9% at − 0.3 V versus RHE in 0.1 M Na_2SO_4, surpassing most MOF based catalysts (Fig. 11d, e). Additionally, Ling's group reported polycrystalline zeolitic imidazolate frameworks (ZIF) layer on the Pt nanosphere-deposited Au electrode [154]. The ZIF layer played three main roles: 1) stimulating the electron-deficient catalytic sites to regulate the D-band of Pt/Au, 2) act as a hydrophobic layer to block the water, 3) enhancing the adsorption N_2 molecules. The designed Pt/Au@ZIF achieved a high NH_3 yield of > 161 μg h^{-1} $mg_{cat.}^{-1}$ and FE of > 44% at ambient conditions, being superior to other Au-Pt electrocatalysts without ZIF (Fig. 11f, g). Recently, other MOF-based composites, such as PdCu@UiO-S@PDMS [160], Au/ZrO_2 [179], Mo-based ZIF-8 derivatives [180], Ag-Au@ZIF [155], ZIF-67 @Ti_3C_2 [181], MoS_2 @ZIF-71 [157], CNT/NCNT@UiO-66 [158], MIL-101(Fe)/MoS_3 [159], Pd/HKUST-1 [182] have also been developed for electrocatalytic NRR. In general, incorporating MOFs into other active materials will blend the benefits of each other, thereby showing great potentials for efficiently electrocatalytic N_2-to-NH_3.

4.1.2. NO_3^-RR/NO_2^-RR

Conductive MOF materials, with dispersed planar metal nodes and unique π-conjugated structures, are promising encapsulates to confine small metal species and protect metal species from aggregation [183]. Lu et al. first developed the conductive copper-based MOF (CuHHTP,

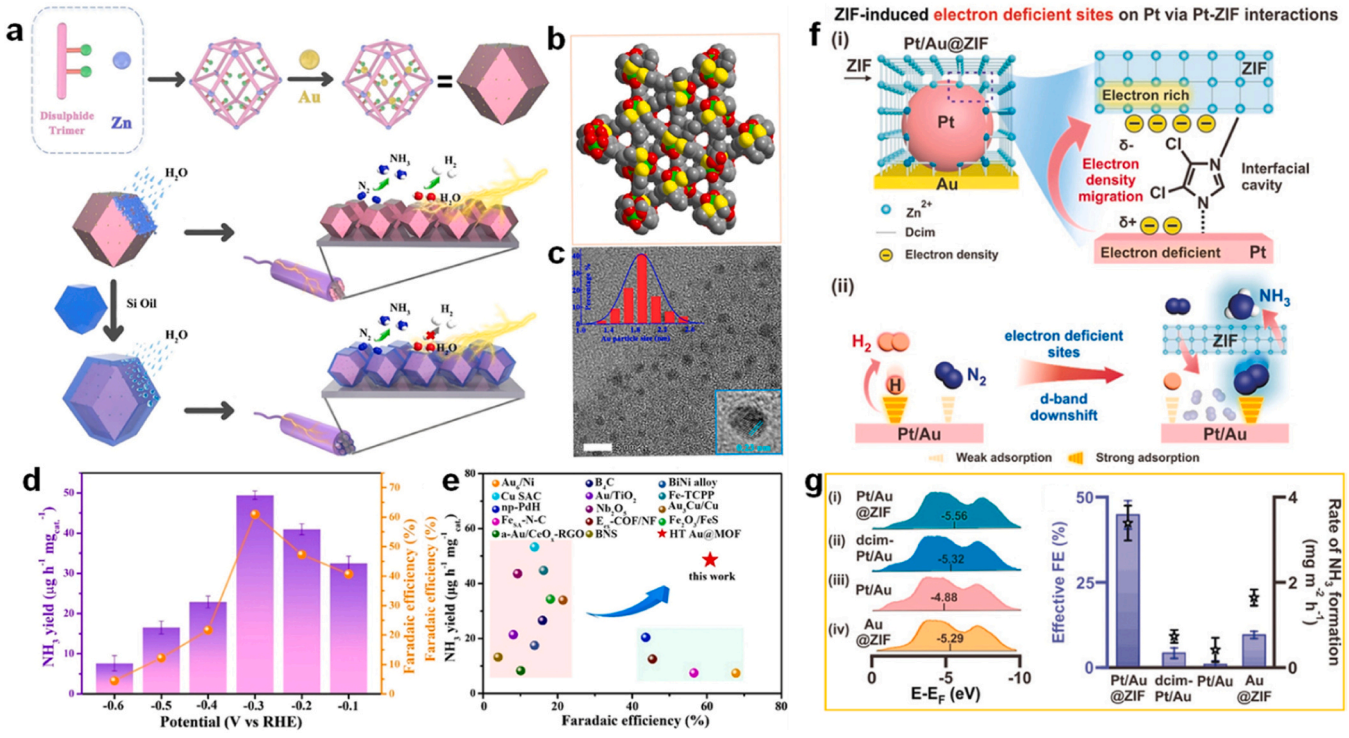

Fig. 11. (a) Schematic depicting a hydrophobic Au@MOF for the electrocatalytic NRR, (b) The 3D crystal structure of Au@MOF, (c) TEM images of Au@MOF with the size distribution of Au NPs, (d) NH_3 yield and FE at different potentials, (e) A comparison of NRR performances of NH_3 yield and FE for HT Au@MOF with other reported materials. (f) Schematic illustration of the function of ZIF, (g) Evaluation of D-band position and corresponding effective FE and rate of ammonia formation for each system, respectively.
Reproduced with permission [153]. Copyright 2022, Elsevier. Reproduced with permission [154]. Copyright 2020, Wiley-VCH.

HHTP = 2,3,6,7,10,11-hexahydroxytriphenylene) nanorods for electrocatalytic nitrate reduction [167]. During the electrochemical NO_3^- reduction process, the CuHHTP nanorods were in situ reduced into metallic Cu clusters confined in the CuHHTP (Cu@CuHHTP, Fig. 12a). The in situ generated Cu@CuHHTP exhibited superb performance for nitrate electroreduction: a high NO_3^- conversion of 85.81% and 96.84% selectivity for NH_3 (Fig. 12b). From the density functional theory (DFT) calculations results, there is 0.57 e^- transferred from CuHHTP to NO_3 * species, which less than that on Cu (111) (0.70 e^-, Fig. 12c, d), indicating the stronger interaction between Cu(111) and NO_3 * . Additionally, the 3d orbit of Cu can not only obtain electrons but also lose electrons, and this "accept−donate" mechanism is more favorable for the adsorption of reaction intermediates. Both the higher ε_d and the "accept−donate" mechanism in charge transfer for Cu(111) ensure the high performance of Cu@CuHHTP (Fig. 12e, f). Considering that EAS from nitrate is highly dependent on the coupling reaction of nitrate and water, interfacial engineering is anticipated to promote the deoxygenation and hydrogenation of nitrate with water. Zhuo et al. developed the hybrid NiCoBDC@HsGDY nanoarray by engineering the surface of bimetallic Ni/Co-MOFs (NiCoBDC) with hydrogen-substituted graphdiyne (HsGDY) for promoting EAS performance [168]. The preparation process of NiCoBDC@HsGDY nanowire array was displayed in Fig. 12g. The decoration of HsGDY on the surface of NiCoBDC facilitates both electrons and NO_3^- ions gathering between NiCoBDC and HsGDY, thus converting rate-determining step and further promoting the efficiency of EAS (Fig. 12h, i). Similarly, they also explored a suite of Cu-MOF hybrid nanoarrays encapsulated with HsGDY tubular shells as effective electrocatalysts for selective nitrate-to-ammonia conversion and achieved good result [169]. Additionally, most state-of-the-art electrocatalysts achieved high NO_3^-RR efficiencies in neutral or alkaline electrolytes, while Ding and coworkers successfully developed a series of Fe_2M (M = Fe, Co, Ni, Zn) trinuclear cluster MOFs that enable the highly efficient electrocatalytic NO_3^-RR to NH_4^+ under strong acidic conditions [172]. Fig. 13a showed 3D framework of Fe_2M-MOF with different trinuclear metal clusters and the tetrakis(1,1'-biphenyl-4-carboxylic acid)− 1, 4-benzenediamine (H_4TPBD) ligand, in which each H_4TPBD ligand is linked to four Fe_2M clusters. Electrochemical NO_3^-RR performance of different Fe_2M-MOFs was systematically evaluated in 0.05 M H_2SO_4 (pH = 1) with 50 g L^{-1} KNO_3 electrolytes. From the linear sweep voltammetry (LSV) curves (Fig. 13b), we can see the NO_3^-RR activities of Fe_2M-MOFs can be summarized as Co > Fe > Ni > Zn. And Fe_2Co-MOFs also showed the best average NH_3 yield rates and the corresponding FEs-NH_3 in the range of 15–100 g L^{-1} KNO_3 (Fig. 13c). DFT computations results indicated that the best performance of Fe_2Co-MOFs could be attributed to the lowering the energy consumption of the NO_3^- adsorption and NO hydrogenation steps (Fig. 13d). And during the electrochemical process, two quasi-reversible single-electron processes were observed in Fe_2Co-N_2-MOF (with H_4TPBD ligand), which can be attributed to $N/N^+/N^{2+}$ redox couples (Fig. 13e). This pioneering work provides new insights into the design principles of high-performance NO_3^-RR catalysts under strong acidic conditions.

Benefited from the high specific surface area, the conductive MOF materials also were applied as the support materials for the post-prepared active materials for electrochemical nitrate reduction to ammonia. For example, Jin and colleagues load the uniform noble metal nanodots (M-NDs, M = Pb, Ag, Au) on the stable and conductive Zr-MOF [170]. The good conductivity of Zr-MOF can facilitate the mass transfer process. Among M-NDs/Zr-MOF materials, Pd-NDs/Zr-MOF exhibited the best activity with a NH_3 yield of 287.31 mmol h^{-1} g^{-1} and a FE of 58.1% (Fig. 14a, b). In addition, Ye and coworkers reported Ru_xO_y clusters stabilized on RuNi-MOFs for ammonia synthesis from nitrate [171]. Fig. 14c is the preparation process, and the RuNi-MOFs exhibited nearly 100% NH_4^+ selectivity (Fig. 14d). From these works, it can be found that MOFs may be a good supporter for active catalysts benefited the dispersion, stabilization and synergistic effect.

4.1.3. NORR

Benefitted from the porous structures, MOFs are expected to act as efficient electrocatalysts for gaseous NO_x pollutant to NH_3. Although no experimental study of MOF materials for NO_x reduction have been reported, Li et al. conducted the DFT calculations of A 2D MOF with hexaaminobenzene (HAB) ligands (TM-HAB MOF, TM = Ti, V, Cr, Mn, Fe, Co, Ni, Cu, Mo, Ru, Rh and Pd) as an electrocatalyst for electrochemical NO to NH_3 [184]. Among the mentioned metal-based MOF

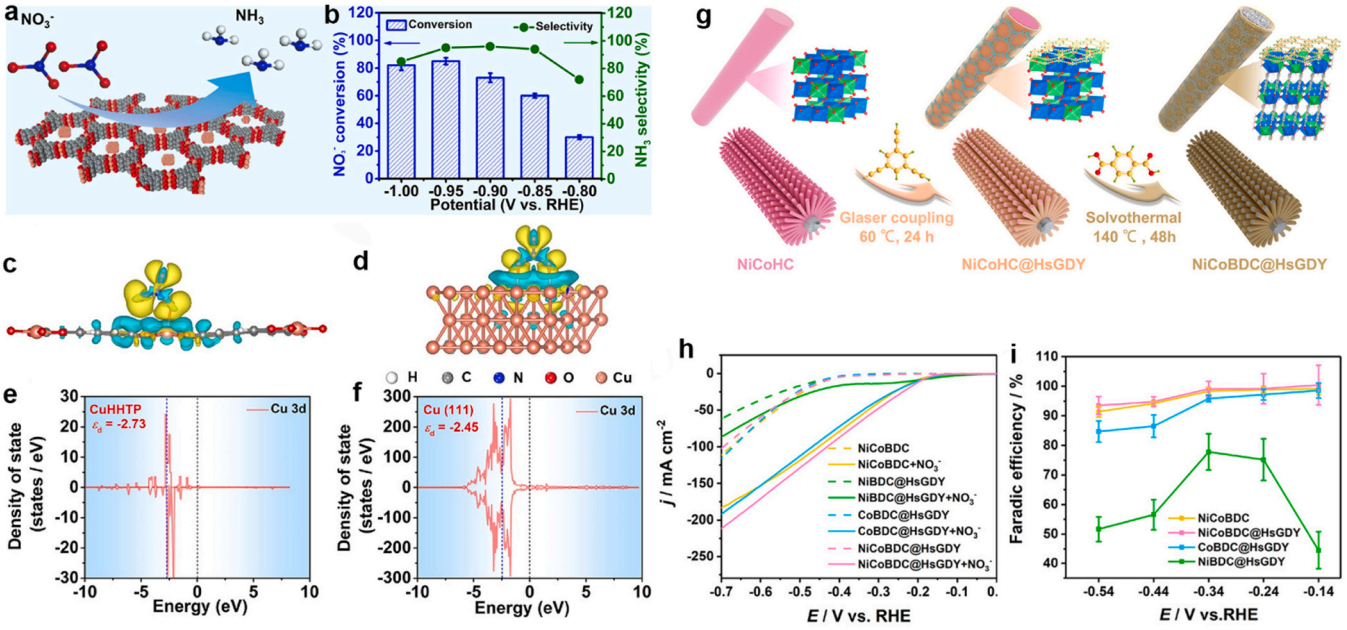

Fig. 12. (a) Schematic diagram of Cu@CuHHTP for NO_3^-RR, (b) NO_3^- conversion and NH_3 selectivity over Cu@CuHHTP, Charge density difference of NO_3 * adsorption on (c) CuHHTP and (d) Cu(111), Density of states for (e) CuHHTP and (f) Cu(111), (g) Schematic illustration for the preparation of NiCoBDC@HsGDY nanowire array, (h) LSV curves of different samples in 1 M KOH with and without 0.1 M NO_3^-, (i) Potential-dependent FEs of different samples
Reproduced with permission [167]. Copyright 2022, American Chemical Society. Reproduced with permission [168]. Copyright 2023, American Chemical Society.

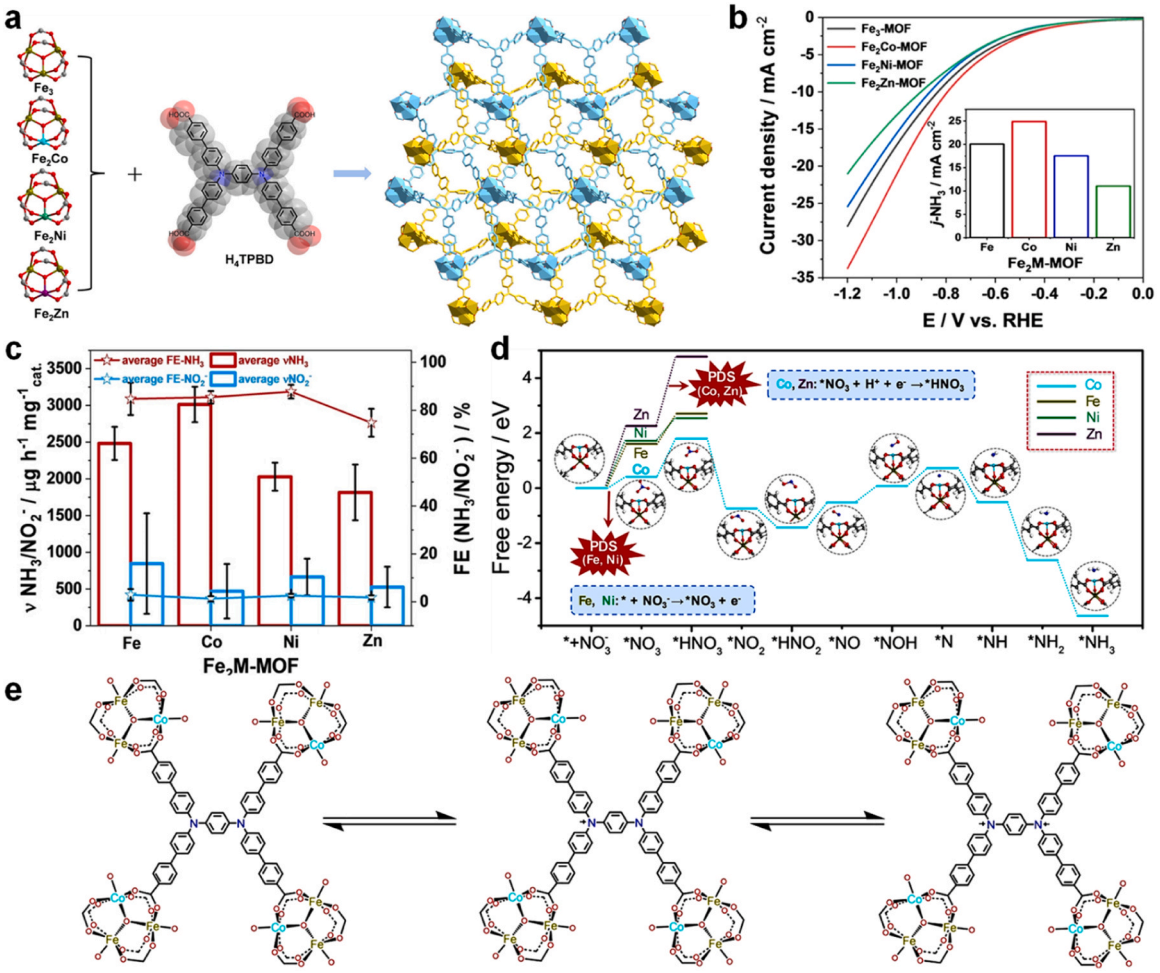

Fig. 13. (a) 3D framework of Fe_2M-MOF with different trinuclear metal clusters and the H_4TPBD ligand, (b) LSV curves of Fe_2M-MOFs in 0.05 M H_2SO_4 (pH = 1) with 50 g L^{-1} KNO_3 electrolytes (inset depicts the partial current densities of ammonia production at −1.1 V_{RHE}), (c) The average NH_3 yield rates and the corresponding FEs-NH_3 of Fe_2M-MOFs at − 1.1 VRHE in 0.05 M H_2SO_4 electrolyte (pH = 1) with the range of 15–100 g L^{-1} KNO_3, (d) Free energy diagram and PDS of electrochemical conversion from NO_3^- to NH_3 in Fe_3, Fe_2Co, Fe_2Ni, and Fe_2Zn systems, (e) Schematic diagram of the different redox states of the nitrogen containing H_4TPBD ligand, where the nitrogen atoms promote both the redox transition (electron transfer) and protonation within the Fe_2Co-N_2-MOF structure. Reproduced with permission [172]. Copyright 2023, Wiley-VCH.

materials, the suitable candidates are Co- and Rh-HAB MOFs due to moderate binding strength between NO and substrates (Fig. 15a, b). Fig. 15c, d show all intermediates of electrochemical NO reduction catalyzed by Co−HAB and Rh−HAB monolayers, and the optimal reaction pathway, respectively. From the theoretical analysis, it can be found that the hydrogenation of NO for ammonia synthesis is feasible at low NO coverage, especially for Co−HAB MOF with low potential and high selectivity. These theoretical results offer the scientific guidance for the design and development of high-efficiency catalysts for electrochemical NO to ammonia.

4.2. MOF derivatives

In view of the depressed conductivity and stability of most MOFs, high-temperature carbonization of MOFs to synthesize MOF derivatives, such as heteroatom-doped porous carbon-based materials, metal/metal compounds and single-metal-atom catalysts, has caught more attention for developing excellent electrocatalysts for EAS via ERRs from various nitrogen sources.

4.2.1. NRR

Heteroatom in porous carbon can not only increase the active sites but also introduce carbon defects and charge polarization of the carbon material, thereby facilitating nitrogen activization. Zhao and coworkers reported N-doped porous carbon (NPC) catalysts synthesized via pyrolysis of ZIF-8 at 750 °C (NPC-750), 850 °C (NPC-850), 950 °C (NPC-950) for electrocatalytic NRR (Fig. 16a) [211]. From both theoretical and experimental tests, the NPC-750 possessed the highest pyridinic and pyrrolic N content of 13.6 at% compared with NPC-850 (5.5 at%) and NPC-950 (2.1 at%), which can promote producing carbon defects and be the active sites for N_2 molecule adsorption and activation. So, the NRR catalytic property of NPC-750 was distinctly better than those of NPC-850 and NPC-950 at − 0.7 and − 0.9 V vs. RHE (Fig. 16b, c). Except for the NPC, N, P co-doping carbon [212], S/NMPC [185] derived from MOFs have also been explored for NRR.

Reasoned from core component of the metal center, MOFs can be converted into metals and metal oxide/phosphide/chalcogenide via the pyrolysis process, which also possess high porosity and plenty of active sites. And the feasibility of introducing multiple metals into MOF materials as precursors can increase the number of actives sites or the synergistic effect for electrocatalytic applications. So, MOF-derived metal/metal compounds have caught much attention as efficient electrocatalysts for NRR. In 2019, metallic Co encapsulated in N doped carbon (Co@NC), which was derived from ZIF-67, was synthesized by Yin's group [186]. The Co@NC acted as electrocatalyst for NRR achieved an excellent performance (NH_3 yield of 1.57×10^{-10} mol s^{-1} cm^{-2}

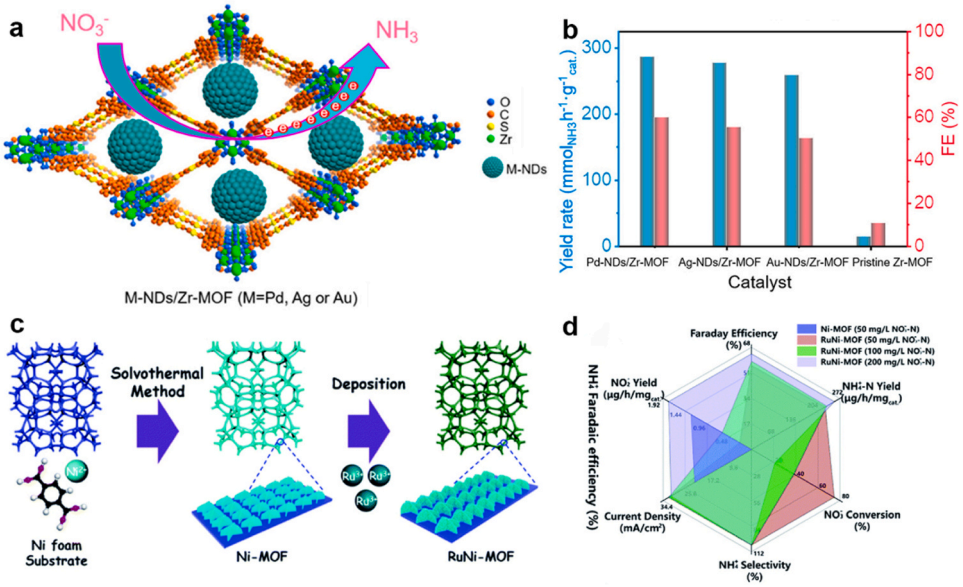

Fig. 14. (a) Schematic diagram of M-NDs/Zr-MOF for NO_3^-RR, (b) Comparison of the NH_3 yields and FE values of different catalysts at − 1.3 V vs. RHE, (c) Schematic illustration of the preparation of the RuNi-MOF catalyst, (d) Comparison of the catalytic performances between the Ni-MOF and RuNi-MOF.
Reproduced with permission [170]. Copyright 2022, American Chemical Society. Reproduced with permission [171]. Copyright 2022, Royal Society of Chemistry.

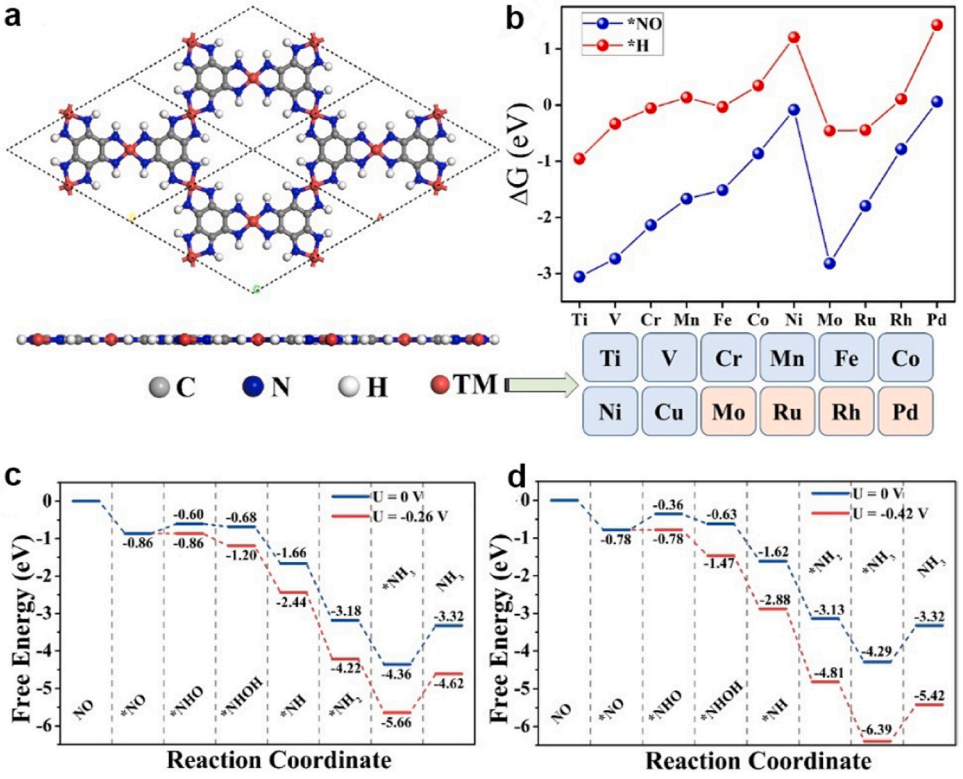

Fig. 15. (a)Top and side views of the HAB monolayer, (b) Adsorption Gibbs free energies for *NO and *H on various HAB monolayers, the TM atom in shaded blue and brown box can be classified into two kinds: the fourth periodic TM and the fifth periodic TM, respectively, Free-energy diagrams for NO reduction on (c) Co-HAB and (d) Rh-HAB MOFs at zero and limiting potential.
Reproduced with permission [184]. Copyright 2021, Wiley-VCH.

and FE value of 21.79% at −0.9 V vs. Ag/AgCl). Except for the original metal species, the MOF derived metal/carbon can be employed as a template for constructing metal-doped carbon. As shown in Fig. 17a, b, Ru NPs dispersed on N-doped carbon materials were fabricated via the carbonization of Ru-doped ZIF-8 with different Ru amounts (denoted as NC@Ru-1, NC@Ru-3, NC@Ru-5,) [187]. From the transmission electron microscope (TEM) images, Ru NPs were dispersed on the retained separate lamellar framework structure. While the NC@Ru hybrids and NC were used for electrocatalytic N_2-to-NH_3, NC@Ru-5 displayed the best performance at − 0.4 V vs. RHE in 0.1 M KOH electrolyte (NH_3 yield of 16.68 μg h^{-1} $mg_{cat.}^{-1}$ and FE of 14.23%) (Fig. 17c, d). This work provides a feasible approach to prepare dispersed noble metal on carbon

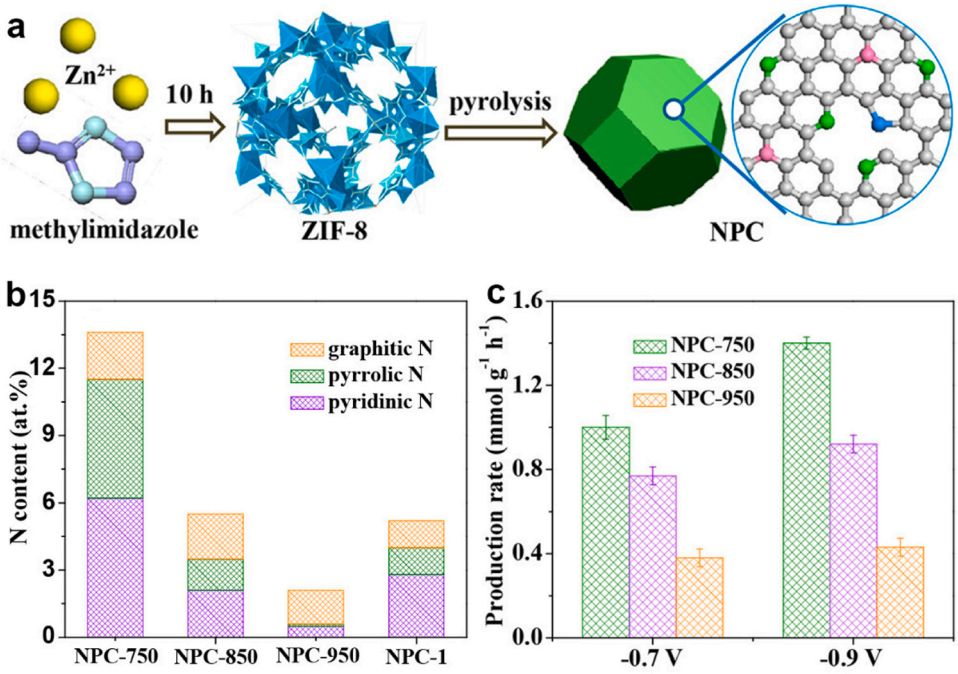

Fig. 16. (a) Schematic illustration of NPC preparation, (b) Contents of pyridinic, pyrrolic, and graphitic N in NPCs, (c) Ammonia production rates of NPC-750, NPC-850, and NPC-950 at − 0.7 and − 0.9 V vs. RHE
Reproduced with permission [211]. Copyright 2018, American Chemical Society.

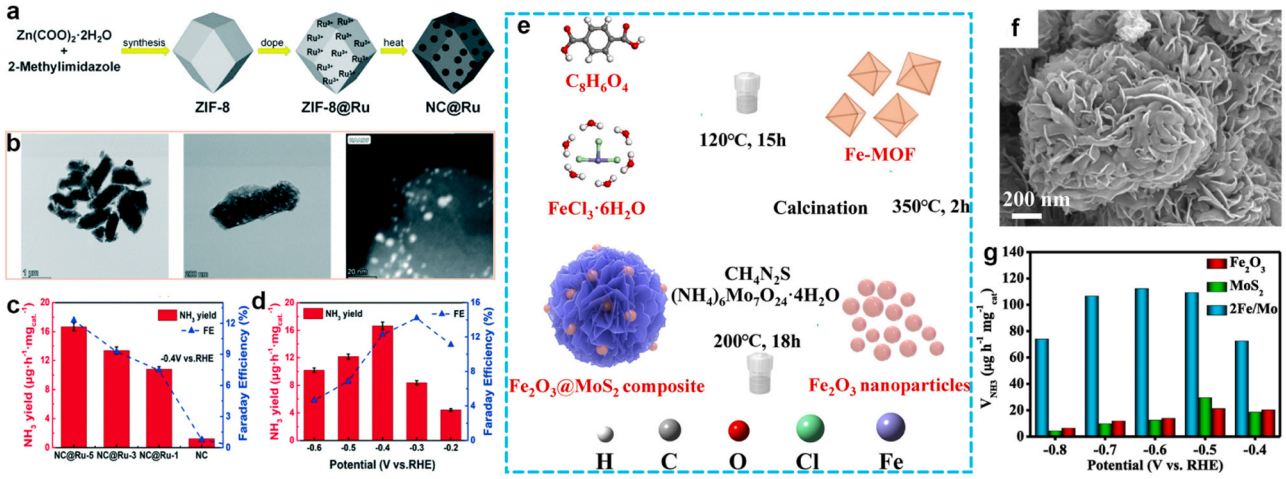

Fig. 17. (a) The synthetic process of NC@Ru. (b) TEM images and high-angle annular dark field scanning transmission electron microscopy (HAADF-STEM) of NC@Ru-3, (c) NH_3 yields and FEs of different catalysts, (d) FEs of NC@Ru at different applied potentials. (e) The synthetic approach of Fe_2O_3/MoS_2, (f) Scanning electron microscopy (SEM) image of Fe_2O_3/MoS_2, (g) NH_3 yields of different samples.
Reproduced with permission [187]. Copyright 2020, Royal Society of Chemistry. Reproduced with permission [188]. Copyright 2022, Elsevier.

for promoting NRR activity. To further improve the catalytic activity of the derived metal, introducing foreign metal to modulate the surface charge distribution and surface structure is a good strategy. W. Huang et al. prepared CoRu@NC through encapsulating ruthenium atoms into ZIF-67 precursor, which exhibited outstanding electrocatalytic NRR activity: an NH_3 yield of 56.82 μg h^{-1} $mg^{-1}_{cat.}$ and FE of 2.02% at − 0.3 V vs. RHE in 0.1 M KOH [189]. Except for the metal, some MOF-derived metal compounds have been also developed as efficient electrocatalysts for NRR. For example, MOF-derived Fe_2O_3 @MoS_2 was reported by Ma's group recently [188]. The Fe_2O_3 @MoS_2 composite was prepared through adding the Fe-MOF derived Fe_2O_3 particles to the synthetic process of MoS_2 (Fig. 17e). From the SEM images, we can see the Fe_2O_3 NPs were anchored on the surface of nanoflower-shaped MoS_2 (Fig. 17f). Electrochemical tests indicate that Fe_2O_3 @MoS_2 achieves an outstanding NH_3 yield of 112.15 μg h^{-1} $mg^{-1}_{cat.}$ at − 0.6 V vs. RHE and a high FE of 8.62% at − 0.4 V vs. RHE in 0.1 M Na_2SO_4, much better than those of the separate MoS2 and Fe_2O_3 (Fig. 17g). The excellent performance of the Fe_2O_3 @MoS_2 can be ascribed to the synergistic effect of Mo and Fe catalytic sites that activated N_2 with a low energy barrier. Very recently, Dai et al. developed TiO_2/CeO_2 framework with plentiful oxygen vacancies based on Ti-based MOFs MIL-125-NH_2 for electrochemical NRR. The unique porous framework and hetero-interfaces collectively facilitated the adsorption/activation of N_2 and mass transfer [190].

Another very important kind of MOF derivatives is MOF-derived single-metal-atom catalysts (SACs) due to the high utilization of the

metallic catalytic site. And MOF materials are attractive precursors for preparing the dispersed SACs due to the adjustable and high dispersed metal center and the isolated metal atoms can be well stabilized by heteroatom and/or the defective sites derived from the MOF precursors. In 2018, Zeng's group first reported Ru single atoms distributed on nitrogen-doped carbon (Ru SAs/N-C) with a record-high activity for electrocatalytic N_2 reduction [191]. As showed in Fig. 18a, the Ru SAs/N-C with the Ru mass loading of 0.18% was synthesized via pyrolyzing the Ru-containing derivative of ZIF-8 at 900 ℃ in N_2 atmosphere. The morphology of the Ru SAs/NC was irregular polyhedrons and the highly dispersive Ru atoms on the N-doped carton could be seen clearly (Fig. 18b-d). Electrocatalytic measurements demonstrate the Ru SAs/N-C showed much better activity for NRR than the Ru NPs/N-C and achieved a record-high yield rate of 120.9 μg h^{-1} $mg_{cat.}^{-1}$ at − 0.2 V vs. RHE with the FE of 29.6% (Fig. 18e). Later, Jiang and co-authors developed the non-noble metal SAs of Fe_1-N-C via using the PCN-222 (Fe) as template during pyrolysis (Fig. 18f) [192]. From the aberration-corrected HAADF-STEM image, many isolated bright spots were found clearly in the Fe_1-N-C, suggesting the well dispersion of Fe atoms (Fig. 18g). The Fe contents in Fe_1-N-C was 1.71 wt%. The Fe_1-N-C achieved the NH_3 production rate of 1.57 × 10^{-10} mol s^{-1} cm^{-2} and FE of 4.51% at a low potential of − 0.05 V vs. RHE (Fig. 18h). These studies offer a meaningful guideline for synthesizing atomically dispersed metal catalysts through the aftertreatment of MOF precursors for efficiently electrochemical N_2 conversion to NH_3 the ambient conditions.

4.2.2. NO_3^-RR/NO_2^-RR

MOFs-derived metal electrocatalysts have attracted most interests for NO_3^-RR/NO_2^-RR due to the intrinsic activity of many metals (Cu, Co, Fe, Ti ect.) [213] and the well dispersion of MOF-derived metals. For example, Sun's team reported the adenine-based MOF derived Co NPs as an attractive electrocatalyst for efficient NH_3 synthesis from nitrate [200]. Geng et al. reported Cu NPs encapsulated with porous carbon framework (denoted Cu@C) for NO_3RR at ultralow concentrations. Owing to the porous structure, NO_3^- could be concentrated in Cu@C, thereby facilitating the mass transfer of NO_3^- with ultralow concentrations [201]. To further improve the active of metallic electrocatalysts, the second metal was proposed to introduced. Xu et al. developed $Cu/Pd/CuO_x$ multi-phase heterostructures through in situ electrochemical reconstitution of Pd-incorporated Cu-based MOF for EAS [203]. The schematic illustration for the preparation of $Cu/Pd/CuO_x$ was showed in Fig. 19a, and the interfaces of Cu and Pd can be clearly observed in the HRTEM image (Fig. 19b, c). Due to the contact and the electronic interaction between Cu, Pd, the electron transferred from Pd to Cu, promoting the nitrate adsorption on electron-deficient Pd sites. And the electron-rich Cu sites further suppressed the competitive HER process. So, the $Cu/Pd/CuO_x$ exhibited the best performance compared with the corresponding contrasts (Fig. 16d, e). Additionally, Dong and co-workers fabricated a series of CuNi alloy NPs with different Cu/Ni ratio embedded in nitrogen-doped carbon matrix through the pyrolysis of Cu, Ni bimetallic MOF materials for high-efficiency electrochemical NO_3^- to NH_3 [205]. The optimized CuNi/NC catalyst (Cu:Ni = 5:1) showed superior performance with the NH_3 selectivity of 94.4% and FE of 79.6% and distinctly alleviate the production of toxic byproduct of nitrite. Recently, Zhang et al. synthesized a series of Ru_xCo_y hollow nanododecahedrons (HNDs) through the post-treatment of dodecahedral ZIF-67 (Fig. 19f, g) [204]. The LSV curves indicated $Ru_{15}Co_{85}$ HNDs exhibit the highest current density at the present of NO_3^- (Fig. 19h). A novel three-step relay mechanism of nitrate reduction over $Ru_{15}Co_{85}$ was proposed to overcome the issue that the high reaction overpotential was needed over most electrocatalysts. During NO_3^-RR, the three-step relay processes that involve spontaneous redox between Co and NO_3^-,

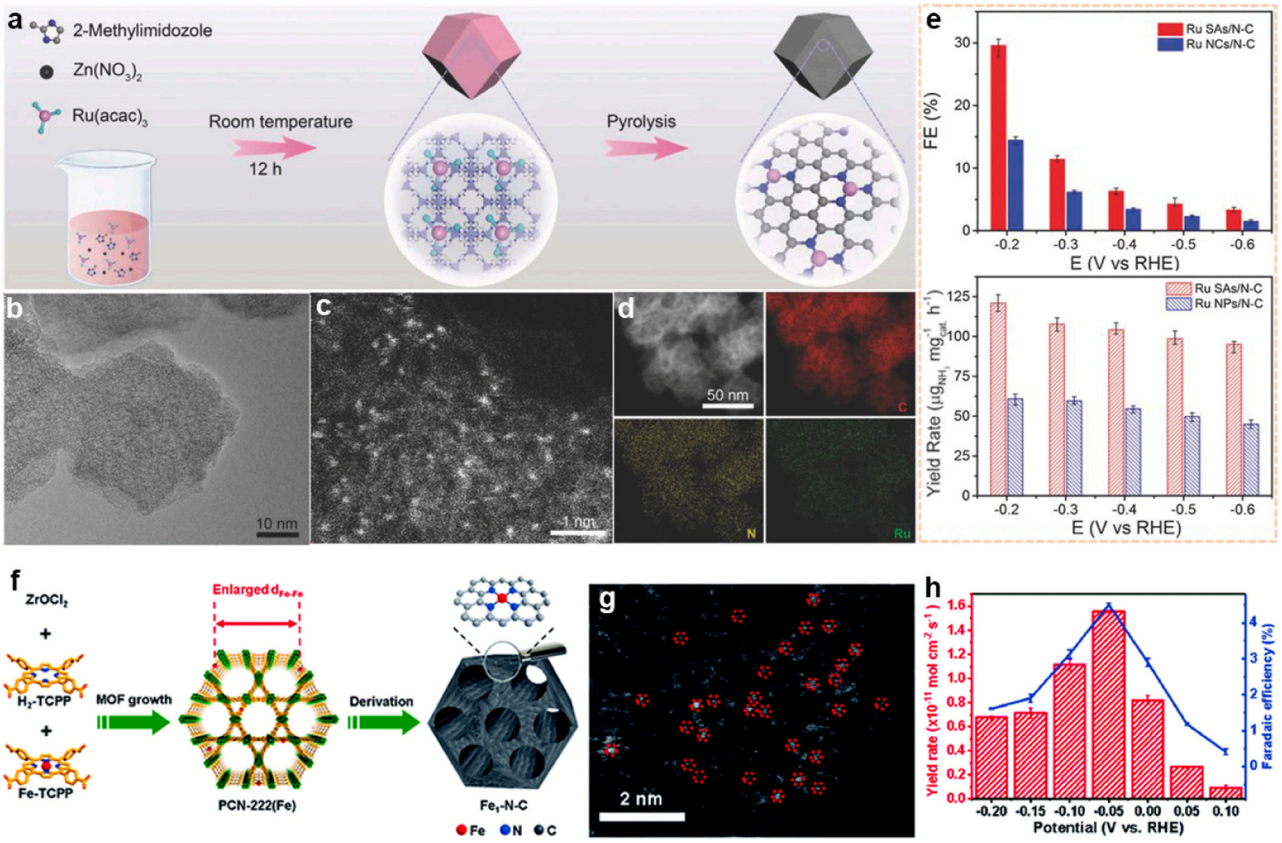

Fig. 18. (a) The synthetic strategy of Ru SAs/NAC, TEM (b), HAADF-STEM (c) and corresponding elemental mapping (d) of Ru SAs/NAC, (e) FEs and NH_3 yield rates of Ru SAs/NAC and Ru NPs/NAC (f) Schematic diagram of Fe_1-N-C derived from PCN-222(Fe), (g) HAADF-STEM images of Fe_1-N-C, (h) NRR properties of Fe_1-N-C (a-e) Reproduced with permission [191]. Copyright 2018, Wiley-VCH. (f-h) Reproduced with permission [192]. Copyright 2019, Royal Society of Chemistry.

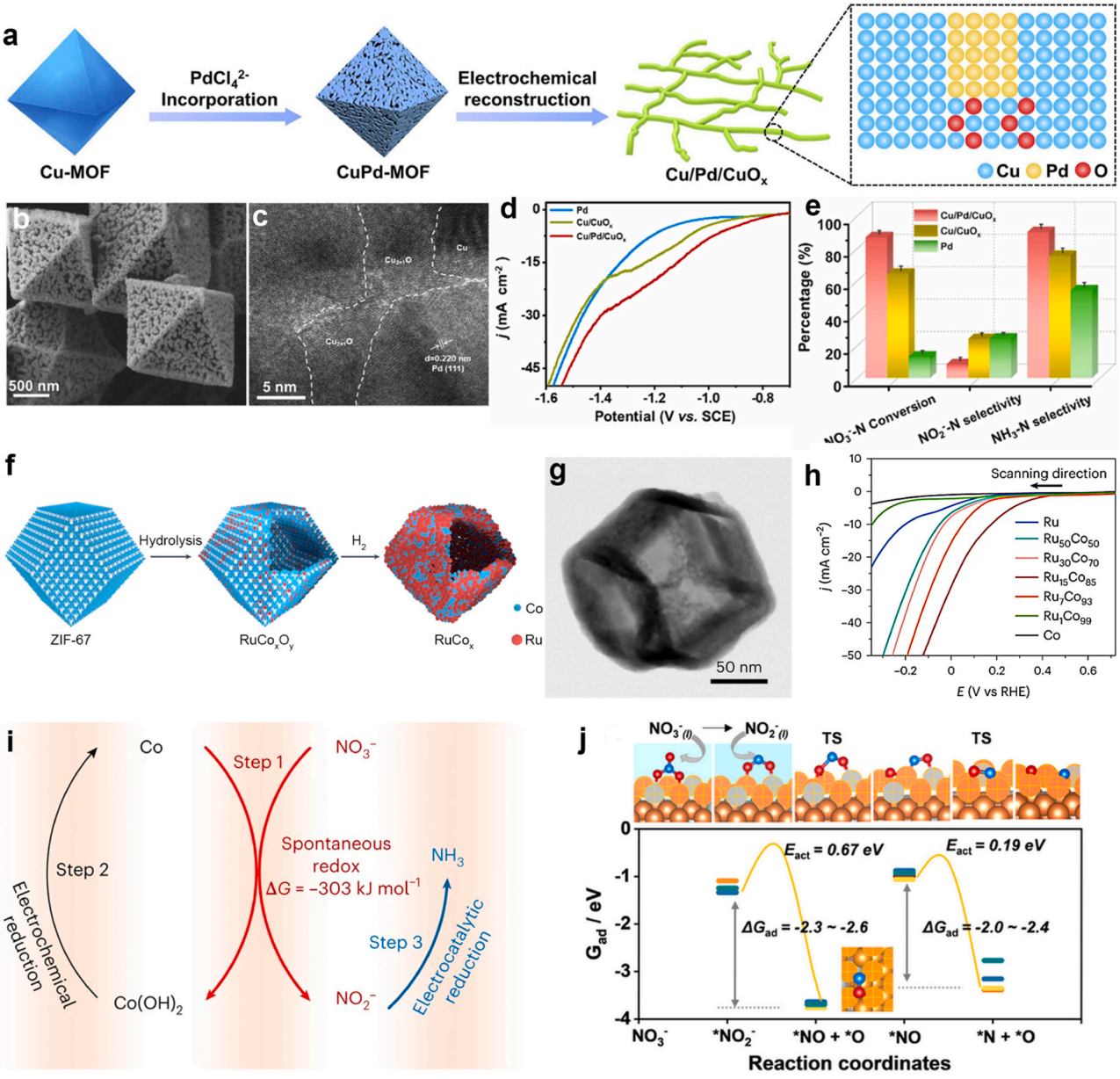

Fig. 19. (a) Schematic illustration of the preparation of Cu/Pd/CuO_x, (b) SEM and (c) HRTEM images of Cu/Pd/CuO_x, (d) LSV curves and (e) NO_3^--N conversion efficiency, selectivity of NH_3-N and NO_2^--N over the Cu/CuO_x, Pd NNs and Cu/Pd/CuO_x, (f) Schematic of Ru_xCo_y HND synthesis, (g) TEM image of $Ru_{15}Co_{85}$, (h) LSV curves for the NO_3^-RR over Ru_xCo_y HNDs under 1600 r.p.m. with 80% iR correction, (i) The three-step relay mechanism for the NO_3^-RR, (j) The activation and reaction energies of the N–O bond-breaking elementary steps
Reproduced with permission [203]. Copyright 2022, Elsevier. Reproduced with permission [204]. Copyright 2023, Nature.

$Co(OH)_2$ electroreduction to Co, and electrocatalytic conversion of NO_2^- to NH_3 occurred (Fig. 19i). The theoretical simulations result of the catalytic reduction of NO_3^- (aq) to NO_2^- (aq) showed that the chemical cleavage of the N–O bond in $*NO_2$ and *NO is thermodynamically highly favoured on $Ru_{15}Co_{85}$ (Fig. 19j).

To improve the atomic utilization of metal catalyst, atomically dispersed metal derived from MOF materials have also been explored for EAS from NO_3^-/NO_2^-. As an example, Xiao et al. prepared atomically dispersed Ru sites loaded on nitrogenated carbon (Ru SA-NC) by a metal organic framework assisted self-assembly process (Fig. 20a, b) [206]. The authors declared that the isolated Ru sites could promote the potential rate-limiting step of *NO → *NOH process, thus showed maximal FE of 97.8% (NO_2^- to NH_3) and 72.8% (NO_3^- to NH_3) toward at − 0.6 and − 0.4 V vs. RHE, respectively, significantly higher than those of Ru NPs (Fig. 20c). Apart from the noble metal, atomically dispersed transition metal was fabricated through post-treatment of MOF materials for nitrate reduction. Ye and coworkers prepared atomically dispersed Cu sites on dual-mesoporous N-doped carbon matrix (Cu−N − C) by a pyrolysis treatment of $Cu(acac)_2$ @ZIF-8 for efficient EAS from nitrate [207]. Furthermore, two atomically dispersed transition metals were also successfully synthesized from corresponding MOF materials. Due to the in situ-trap Cu and Ni precursors in the cages of ZIF-8 during crystallization, Cu and Ni dual-single-atom into nitrogen-doped carbon was obtained after the pyrolysis of Cu^{2+}, Ni^{2+} filled ZIF-8 (Fig. 20d) [208]. The prepared Cu/Ni-NC with dual active sites shows the higher FEs (97.28%) and selectivity (94.84%) of NH_3 during nitrate reduction compared with Cu–NC and Ni–NC. The superior performance of Cu/Ni-NC was mainly attribute to two factors: (i) the strong hybridizations of Cu 3d − Ni 3d − O 2p orbitals of NO_3^- can accelerate electron transfer from Cu–Ni dual-site to NO_3^-, (ii) Cu/Ni–NC can not only

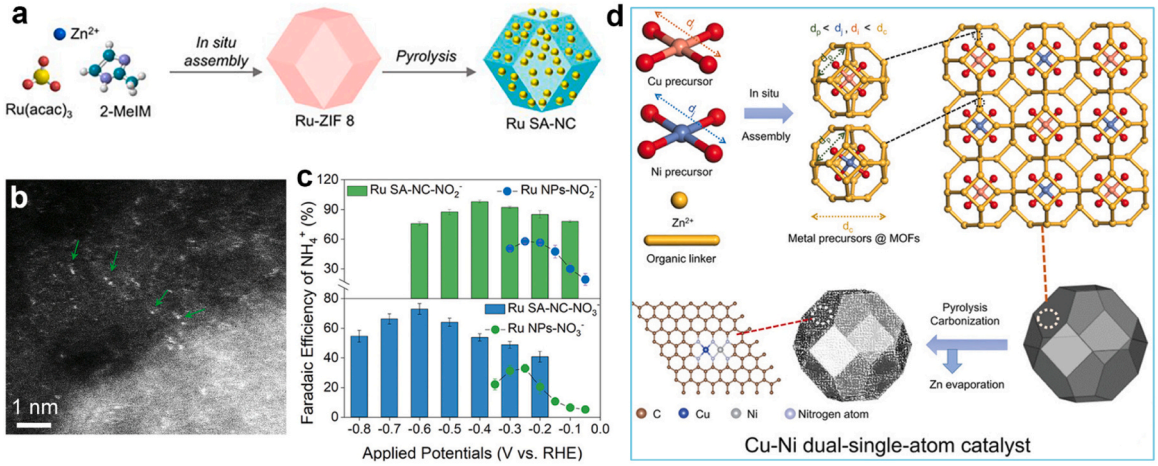

Fig. 20. (a) Illustration of Ru SA-NC synthesis, (b) HAADF-STEM image, (c) FEs of NH_3 from NO_3^- and NO_2^- reduction over Ru SA-NC and Ru NPs (d) Schematic illustration of the synthetic procedure of Cu/Ni–NC.
(a-c) Reproduced with permission [206]. Copyright 2023, American Chemical Society. (d) Reproduced with permission [208]. Copyright 2023, Wiley-VCH.

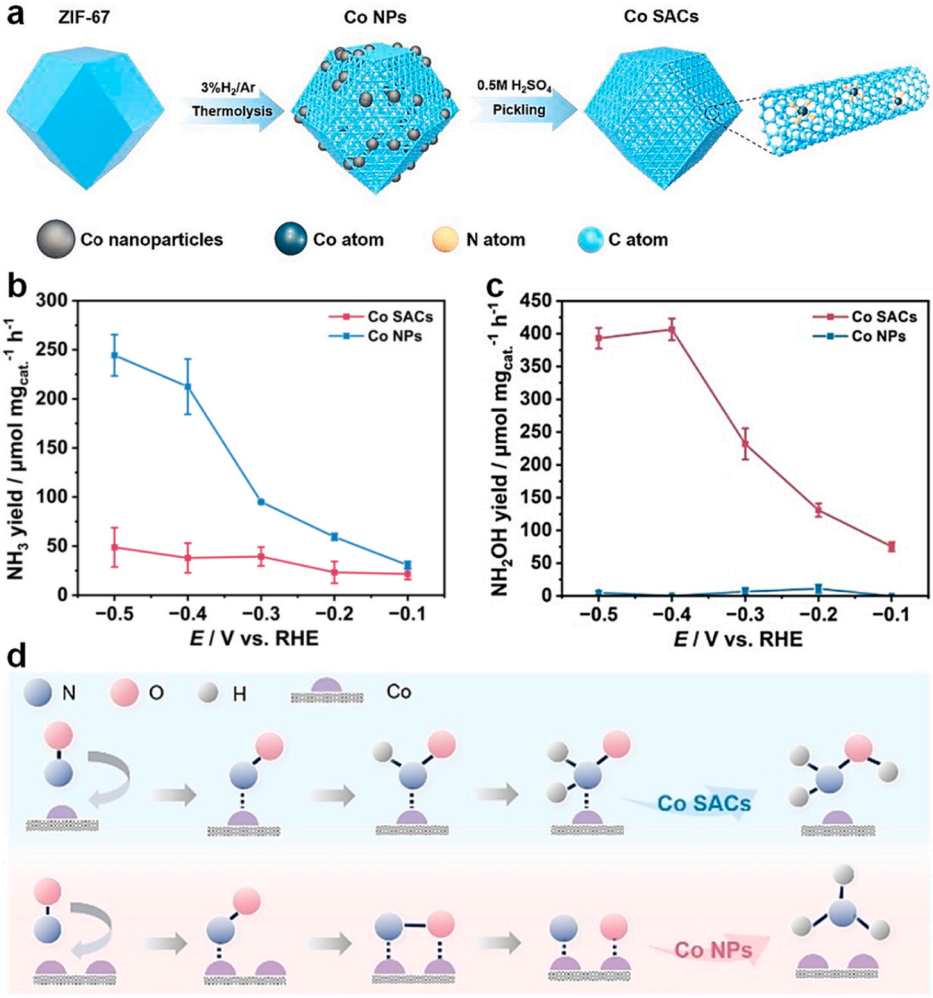

Fig. 21. (a) Schematic illustration of the preparation of Co SACs and Co NPs, (b) Yield rate of NH_3 on Co SACs and Co NPs at each given potential, (c) Yield rate of NH_2OH on Co SACs and Co NPs at each given potential, (d) Deduced electrocatalytic NORR pathway on Co SACs and Co NPs for the production of NH_2OH and NH_3, respectively.
Reproduced with permission [210]. Copyright 2023, Wiley-VCH.

decrease barrier of the rate-limiting step but also suppress N-N coupling for N_2O and N_2 formation and HER.

4.2.3. NORR

Currently, the development of MOFs-derived electrocatalysts for EAS from NOx is still in initial stage. Very recently, Zhang and coworkers developed ZIF-67 derived Co electrocatalysts for electrocatalytic NORR [210]. The product selectivity of NORR over different Co catalysts was studied in-depth. Concretely, Co SACs and Co NPs were prepared by the facile chemical conversion of ZIF-67 precursor and the schematic diagram of the synthesis process was showed in Fig. 21a. When the Co SACs and Co NPs were applied as the electrocatalysts for NORR, they showed quite different selectivity of the production. As shown in Fig. 21b, c, For Co NPs, the main product was NH_3, but Co SACs selectively produced hydroxyl amine (NH_2OH). In-depth exploration results by the authors unveil that linear adsorption of NO on isolated Co sites enables NH_2OH formation and bridge adsorption of NO on adjacent Co sites induce the production of NH_3 (Fig. 21d). This work provides well scientific guidance to design efficient electrocatalysts for selective NORR to NH_3.

5. Summary and outlook

The EAS is considered as an environmentally friendly alternative to the traditional energy-intensive H−B process. MOF-based materials are a family of promising electrocatalysts that attract great attention to act as electrocatalysts for EAS due to their unique structural merits. In this review, we summarized recent advances of the class of MOFs and their derivatives acted as electrocatalyst for EAS, including the possible mechanism of EAS via ERRs using various nitrogen sources as well as the quantification methods of ammonia, the structural features and merits of MOF-based materials acted as electrocatalysts, and recent advance in NH_3 synthesis from various nitrogen sources under ambient conditions over MOF-based electrocatalysts. The highly diverse and tunable structural/compositional properties endow pristine MOFs/MOF composites excellent electrocatalytic performance for EAS via ERRs using various nitrogen sources. Additionally, these advantageous properties also enable multiple rational design of MOF derivatives with high-active sites, conducive interaction in interfaces/heterostructures, porous structures to achieve a best overall electrochemical performance of ammonia synthesis, as discussed as above sections. To improve the electrocatalytic performances of MOF-based materials, constructing the multiple components with interfaces is an efficient method due to the electronic properties of the active components could be optimized by the interfacial charge redistribution. However, as displayed in Table 1 and Table 2, the NH_3 yield rate and FE, especially using N_2 as nitrogen source, are still lower than the commercially viable targets released by the U. S. Department of Energy (a current density of 300 mA cm^{-2} with a FE of 90% and energy efficiency of 60%) over most of current reported MOF-based electrocatalysts [91]. More efforts to rationally design MOFs-based electrocatalysts and catalytic system with high current density, FE and stability for EAS are anticipated but still challenging.

Based on our current understanding of EAS based on MOFs and their derivatives, a few comments for future research in this field can be suggested.

(1) To achieve the commercially viable targets, constructing of a new type of electrolysis reactor to realize stable and continuous NH_3 production with high current density is important for the practical application of EAS. And the separation and collection technology of ammonia is expected to be integrated to the electrolysis reactor. Additionally, large-scale NO_3^- electroreduction in the actual waste water for NH_3 synthesis to achieve "turn waste into wealth" is still a great challenge due to the fluctuation and complexity (e.g., NO_3^- concentration, pH value, conductivity and interference of impurity ions) of the actual waste water, which requires the ingenious design of the electrocatalysts with selective adsorption, high activity, thermal/chemical stability for the large-scale sewage treatment.

(2) The clear catalytic mechanism of MOFs and their derivatives for EAS via ERRs from various nitrogen sources is essential to elucidate the structure-activity relationship for adequately guiding the rational design of MOFs-based functional materials. The comprehensive utilization of multiple in situ test techniques like diffuse Fourier transform infrared spectrum (DRIFTS), Raman spectrum, differential electrochemical mass spectrometry (DEMS), and electron spin resonance (ESR) spectroscopy combined with X-ray diffraction (XRD), X-ray absorption fine structure (XAFS) and the theoretical calculations is efficient to reveal the accurate catalytical active site and reaction path. Based on the transparent catalytic mechanism, regulating and optimizing the compositions, electronic structures, and coordination environments of MOF based catalysts can efficiently decrease the highest energy barrier of rate-determining step and thus improve the catalytic performance.

(3) The economic efficiency (EE) should be considered as one of the significant indicators of EAS performance evaluation criteria of the catalysts. For the practical application, the final cost of the electrochemical process is highly dependent on energy consumption. So, the less energy the EAS consumes, the more economical it is for sustainable application.

(4) Considering that one of the most important applications of NH_3 is acted as the feedstock for amide chemicals, like urea, formamide and so on, it is fascinating that electrochemically coupling the CO_2 reduction and ammonia synthesis from various nitrogen sources realizes C-N bonding through precise designing MOFs or their derivatives as electrocatalysts.

In summary, MOFs and their derivatives show greatly up-and coming platforms to obtain high-efficiency electrocatalysts for the NH_3 synthesis via different nitrogen sources. But the current research is still in the preliminary theoretical stage and far from the standard of practical application. More efforts from chemists, electrochemists, material scientists, and chemical engineers are needed to store the renewable energy and reduce the energy consumption and CO_2 emissions of the NH_3 industry synthesis.

Declaration of Competing Interest

The authors declare that they have no known competing financial interests or personal relationships that could have appeared to influence the work reported in this paper.

Data Availability

No data was used for the research described in the article.

Acknowledgements

We acknowledge the National Natural Science Foundation of China (U21A20286 and 22206054), Natural Science Foundation of Hubei (ZRMS2021000800), the Fundamental Research Funds for the Central China Normal University (CCNU) and the research start-up fund from Anhui University (S020318008/015) for financial support.

References

[1] J.G. Chen, R.M. Crooks, L.C. Seefeldt, K.L. Bren, R.M. Bullock, M.Y. Darensbourg, P.L. Holland, B. Hoffman, M.J. Janik, A.K. Jones, M.G. Kanatzidis, P. King, K. M. Lancaster, S.V. Lymar, P. Pfromm, W.F. Schneider, R.R. Schrock, Beyond fossil fuel–driven nitrogen transformations, Science 360 (2018), eaar6611.

[2] B. Yang, W. Ding, H. Zhang, S. Zhang, Recent progress in electrochemical synthesis of ammonia from nitrogen: Strategies to improve the catalytic activity and selectivity, Energy Environ. Sci. 14 (2021) 672–687.

[3] O. Elishav, B. Mosevitzky Lis, E.M. Miller, D.J. Arent, A. Valera-Medina, A. Grinberg Dana, G.E. Shter, G.S. Grader, Progress and prospective of nitrogen-based alternative fuels, Chem. Rev. 120 (2020) 5352–5436.
[4] G. Soloveichik, Electrochemical synthesis of ammonia as a potential alternative to the Haber–Bosch process, Nat. Catal. 2 (2019) 377–380.
[5] L. Wang, M. Xia, H. Wang, K. Huang, C. Qian, C.T. Maravelias, G.A. Ozin, Greening ammonia toward the solar ammonia refinery, Joule 2 (2018) 1055–1074.
[6] M. Wang, M.A. Khan, I. Mohsin, J. Wicks, A.H. Ip, K.Z. Sumon, C.-T. Dinh, E. H. Sargent, I.D. Gates, M.G. Kibria, Can sustainable ammonia synthesis pathways compete with fossil-fuel based Haber–Bosch processes? Energy Environ. Sci. 14 (2021) 2535–2548.
[7] S. Wang, F. Ichihara, H. Pang, H. Chen, J. Ye, Nitrogen fixation reaction derived from nanostructured catalytic materials, Adv. Funct. Mater. 28 (2018) 1803309.
[8] M.C. Hatzell, A decade of electrochemical ammonia synthesis, ACS Energy Lett. 7 (2022) 4132–4133.
[9] M. Nazemi, M.A. El-Sayed, Managing the nitrogen cycle via plasmonic (photo) electrocatalysis: Toward circular economy, Acc. Chem. Res. 54 (2021) 4294–4304.
[10] F. Jiao, B. Xu, Electrochemical ammonia synthesis and ammonia fuel cells, Adv. Mater. 31 (2019) 1805173.
[11] W. Xiong, M. Zhou, H. Li, Z. Ding, D. Zhang, Y. Lv, Electrocatalytic ammonia synthesis catalyzed by mesoporous nickel oxide nanosheets loaded with Pt nanoparticles, Chin. J. Catal. 43 (2022) 1371–1378.
[12] W. Xiong, M. Zhou, X. Huang, W. Yang, D. Zhang, Y. Lv, H. Li, Direct in situ vertical growth of interlaced mesoporous NiO nanosheets on carbon felt for electrocatalytic ammonia synthesis, Chem. Eur. J. 28 (2022), e202200779.
[13] W. Xiong, H. Yin, T. Wu, H. Li, Challenges and opportunities of transition metal oxides as electrocatalysts, Chem. Eur. J. 29 (2023), e202202872.
[14] H. He, H.-M. Wen, H.-K. Li, P. Li, J. Wang, Y. Yang, C.-P. Li, Z. Zhang, M. Du, Hydrophobicity tailoring of Ferric Covalent Organic Framework/Mxene nanosheets for high-efficiency nitrogen electroreduction to ammonia, Adv. Sci. 10 (2023) 2206933.
[15] X. Peng, L. Zeng, D. Wang, Z. Liu, Y. Li, Z. Li, B. Yang, L. Lei, L. Dai, Y. Hou, Electrochemical C–N coupling of CO_2 and nitrogenous small molecules for the electrosynthesis of organonitrogen compounds, Chem. Soc. Rev. 52 (2023) 2193–2237.
[16] Y. Baik, M. Kwen, K. Lee, S. Chi, S. Lee, K. Cho, H. Kim, M. Choi, Splitting of hydrogen atoms into proton–electron pairs at BaO–Ru interfaces for promoting ammonia synthesis under mild conditions, J. Am. Chem. Soc. 145 (2023) 11364–11374.
[17] H. Fei, R. Liu, J. Wang, T. Guo, Z. Wu, D. Wang, F. Liu, Targeted modulation of competitive active sites toward nitrogen fixation via sulfur vacancy engineering over MoS_2, Adv. Funct. Mater. (2023) 2302501.
[18] T.-N. Ye, S.-W. Park, Y. Lu, J. Li, M. Sasase, M. Kitano, T. Tada, H. Hosono, Vacancy-enabled N_2 activation for ammonia synthesis on an Ni-loaded catalyst, Nature 583 (2020) 391–395.
[19] M. Zhou, W. Xiong, H. Li, D. Zhang, Y. Lv, Emulsion-template synthesis of mesoporous nickel oxide nanoflowers composed of crossed nanosheets for effective nitrogen reduction, Dalton T 50 (2021) 5835–5844.
[20] H. Jiang, G.-F. Chen, O. Savateev, J. Xue, L.-X. Ding, Z. Liang, M. Antonietti, H. Wang, Enabled efficient ammonia synthesis and energy supply in a Zinc–Nitrate battery system by separating nitrate reduction process into two stages, Angew. Chem. Int. Ed. 62 (2023), e202218717.
[21] H.-L. Du, M. Chatti, R.Y. Hodgetts, P.V. Cherepanov, C.K. Nguyen, K. Matuszek, D.R. MacFarlane, A.N. Simonov, Electroreduction of nitrogen with almost 100% current-to-ammonia efficiency, Nature 609 (2022) 722–727.
[22] H.-L. Du, K. Matuszek, R.Y. Hodgetts, K. Ngoc Dinh, P.V. Cherepanov, J. M. Bakker, D.R. MacFarlane, A.N. Simonov, The chemistry of proton carriers in high-performance lithium-mediated ammonia electrosynthesis, Energy Environ. Sci. 16 (2023) 1082–1090.
[23] S.Z. Andersen, M.J. Statt, V.J. Bukas, S.G. Shapel, J.B. Pedersen, K. Krempl, M. Saccoccio, D. Chakraborty, J. Kibsgaard, P.C.K. Vesborg, J. Nørskov, I. Chorkendorff, Increasing stability, efficiency, and fundamental understanding of lithium-mediated electrochemical nitrogen reduction, Energy Environ. Sci. 13 (2020) 4291–4300.
[24] N. Lazouski, Z.J. Schiffer, K. Williams, K. Manthiram, Understanding continuous lithium-mediated electrochemical nitrogen reduction, Joule 3 (2019) 1127–1139.
[25] R. Tang, J. Huang, Enclosing the nitrogen cycle: Ammonia synthesis by NO_x reduction, Curr. Opin. Green. Sustain. Chem. 38 (2022), 100681.
[26] H. Zhang, Y. Li, C. Cheng, J. Zhou, P. Yin, H. Wu, Z. Liang, J. Zhang, Q. Yun, A.-L. Wang, L. Zhu, B. Zhang, W. Cao, X. Meng, J. Xia, Y. Yu, Q. Lu, Isolated electron-rich ruthenium atoms in intermetallic compounds for boosting electrochemical nitric oxide reduction to ammonia, Angew. Chem. Int. Ed. 62 (2023), e202213351.
[27] Z. Jiang, Y. Wang, Z. Lin, Y. Yuan, X. Zhang, Y. Tang, H. Wang, H. Li, C. Jin, Y. Liang, Molecular electrocatalysts for rapid and selective reduction of nitrogenous waste to ammonia, Energy Environ. Sci. 16 (2023) 2239–2246.
[28] S.E. Braley, J. Xie, Y. Losovyj, J.M. Smith, Graphite conjugation of a macrocyclic cobalt complex enhances nitrite electroreduction to ammonia, J. Am. Chem. Soc. 143 (2021) 7203–7208.
[29] Y. Zhang, Y. Wang, L. Han, S. Wang, T. Cui, Y. Yan, M. Xu, H. Duan, Y. Kuang, X. Sun, Nitrite electroreduction to ammonia promoted by molecular carbon dioxide with near-unity faradaic efficiency, Angew. Chem. Int. Ed. 62 (2023), e202213711.
[30] D. Liu, L. Qiao, S. Peng, H. Bai, C. Liu, W.F. Ip, K.H. Lo, H. Liu, K.W. Ng, S. Wang, X. Yang, H. Pan, Recent advances in electrocatalysts for efficient nitrate reduction to ammonia, Adv. Funct. Mater. (2023) 2303480.
[31] O.M. Yaghi, H. Li, Hydrothermal synthesis of a metal-organic framework containing large rectangular channels, J. Am. Chem. Soc. 117 (1995) 10401–10402.
[32] M. Zhong, L. Kong, N. Li, Y.-Y. Liu, J. Zhu, X.-H. Bu, Synthesis of MOF-derived nanostructures and their applications as anodes in lithium and sodium ion batteries, Coord. Chem. Rev. 388 (2019) 172–201.
[33] B. Zhu, R. Zou, Q. Xu, Metal–organic framework based catalysts for hydrogen evolution, Adv. Energy Mater. 8 (2018) 1801193.
[34] B. Geng, F. Yan, X. Zhang, Y. He, C. Zhu, S.-L. Chou, X. Zhang, Y. Chen, Conductive CuCo-based bimetal organic framework for efficient hydrogen evolution, Adv. Mater. 33 (2021) 2106781.
[35] W. Cheng, H. Zhang, D. Luan, X.W. Lou, Exposing unsaturated Cu_1-O_2 sites in nanoscale Cu-MOF for efficient electrocatalytic hydrogen evolution, Sci. Adv. 7 (2021), eabg2580.
[36] Y. Sun, Z. Xue, Q. Liu, Y. Jia, Y. Li, K. Liu, Y. Lin, M. Liu, G. Li, C.-Y. Su, Modulating electronic structure of metal-organic frameworks by introducing atomically dispersed Ru for efficient hydrogen evolution, Nat. Commun. 12 (2021) 1369.
[37] D. Yang, Y. Chen, Z. Su, X. Zhang, W. Zhang, K. Srinivas, Organic carboxylate-based MOFs and derivatives for electrocatalytic water oxidation, Coord. Chem. Rev. 428 (2021), 213619.
[38] X.Z. Song, N. Zhang, X.F. Wang, Z. Tan, Recent advances of metal-organic frameworks and their composites toward oxygen evolution electrocatalysis, Mater. Today Energy 19 (2021), 100597.
[39] J. Du, F. Li, L. Sun, Metal–organic frameworks and their derivatives as electrocatalysts for the oxygen evolution reaction, Chem. Soc. Rev. 50 (2021) 2663–2695.
[40] C. Li, Y. Ji, Y. Wang, C. Liu, Z. Chen, J. Tang, Y. Hong, X. Li, T. Zheng, Q. Jiang, C. Xia, Applications of metal–organic frameworks and their derivatives in electrochemical CO_2 reduction, Nano-Micro Lett. 15 (2023) 113.
[41] H. Zhong, M. Ghorbani-Asl, K.H. Ly, J. Zhang, J. Ge, M. Wang, Z. Liao, D. Makarov, E. Zschech, E. Brunner, I.M. Weidinger, J. Zhang, A. V. Krasheninnikov, S. Kaskel, R. Dong, X. Feng, Synergistic electroreduction of carbon dioxide to carbon monoxide on bimetallic layered conjugated metal-organic frameworks, Nat. Commun. 11 (2020) 1409.
[42] X. Xie, X. Zhang, M. Xie, L. Xiong, H. Sun, Y. Lu, Q. Mu, M.H. Rummeli, J. Xu, S. Li, J. Zhong, Z. Deng, B. Ma, T. Cheng, W.A. Goddard, Y. Peng, Au-activated N motifs in non-coherent cupric porphyrin metal organic frameworks for promoting and stabilizing ethylene production, Nat. Commun. 13 (2022) 63.
[43] H. He, H.-M. Wen, H.-K. Li, H.-W. Zhang, Recent advances in metal–organic frameworks and their derivatives for electrocatalytic nitrogen reduction to ammonia, Coord. Chem. Rev. 471 (2022), 214761.
[44] I.E. Khalil, C. Xue, W. Liu, X. Li, Y. Shen, S. Li, W. Zhang, F. Huo, The role of defects in metal–organic frameworks for nitrogen reduction reaction: When defects switch to features, Adv. Funct. Mater. 31 (2021) 2010052.
[45] H. He, H.-K. Li, Q.-Q. Zhu, C.-P. Li, Z. Zhang, M. Du, Hydrophobicity modulation on a Ferriporphyrin-based metal–organic framework for enhanced ambient electrocatalytic nitrogen fixation, Appl. Catal. B Environ. 316 (2022), 121673.
[46] G. Cai, P. Yan, L. Zhang, H.-C. Zhou, H.-L. Jiang, Metal–organic framework-based hierarchically porous materials: Synthesis and applications, Chem. Rev. 121 (2021) 12278–12326.
[47] S. Dang, Q.-L. Zhu, Q. Xu, Nanomaterials derived from metal–organic frameworks, Nat. Rev. Mater. 3 (2017) 17075.
[48] P. Zhou, J. Lv, X. Huang, Y. Lu, G. Wang, Strategies for enhancing the catalytic activity and electronic conductivity of MOFs-based electrocatalysts, Coord. Chem. Rev. 478 (2023), 214969.
[49] Y. Zhang, L. Jiao, W. Yang, C. Xie, H.-L. Jiang, Rational fabrication of low-coordinate single-atom Ni electrocatalysts by MOFs for highly selective CO_2 reduction, Angew. Chem. Int. Ed. 60 (2021) 7607–7611.
[50] H. Yang, X. Wang, Secondary-component incorporated hollow MOFs and derivatives for catalytic and energy-related applications, Adv. Mater. 31 (2019) 1800743.
[51] I.E. Khalil, C. Xue, W. Liu, X. Li, Y. Shen, S. Li, W. Zhang, F. Huo, The role of defects in metal–organic frameworks for nitrogen reduction reaction: When defects switch to features, Adv. Funct. Mater. 31 (2021).
[52] J. Deng, J.A. Iñiguez, C. Liu, Electrocatalytic nitrogen reduction at low temperature, Joule 2 (2018) 846–856.
[53] A.J. Martín, T. Shinagawa, J. Pérez-Ramírez, Electrocatalytic reduction of nitrogen: From Haber-Bosch to ammonia artificial leaf, Chem 5 (2019) 263–283.
[54] Y. Yang, S.Q. Wang, H. Wen, T. Ye, J. Chen, C.P. Li, M. Du, Nanoporous gold embedded ZIF composite for enhanced electrochemical nitrogen fixation, Angew. Chem. Int. Ed. 58 (2019) 15362–15366.
[55] W. Guo, K. Zhang, Z. Liang, R. Zou, Q. Xu, Electrochemical nitrogen fixation and utilization: theories, advanced catalyst materials and system design, Chem. Soc. Rev. 48 (2019) 5658–5716.
[56] G. Qing, R. Ghazfar, S.T. Jackowski, F. Habibzadeh, M.M. Ashtiani, C.P. Chen, M. R. Smith 3rd, T.W. Hamann, Recent advances and challenges of electrocatalytic N_2 reduction to ammonia, Chem. Rev. 120 (2020) 5437–5516.
[57] T.H. Rod, A. Logadottir, J.K. Nørskov, Ammonia synthesis at low temperatures, J. Chem. Phys. 112 (2000) 5343–5347.
[58] H.-P. Jia, E.A. Quadrelli, Mechanistic aspects of dinitrogen cleavage and hydrogenation to produce ammonia in catalysis and organometallic chemistry:

Relevance of metal hydride bonds and dihydrogen, Chem. Soc. Rev. 43 (2014) 547–564.
[59] C.-G. Zhan, J.A. Nichols, D.A. Dixon, Ionization potential, electron affinity, electronegativity, hardness, and electron excitation energy: Molecular properties from density functional theory orbital energies, J. Phys. Chem. A 107 (2003) 4184–4195.
[60] V. Kyriakou, I. Garagounis, E. Vasileiou, A. Vourros, M. Stoukides, Progress in the electrochemical synthesis of ammonia, Catal. Today 286 (2017) 2–13.
[61] I.A. Amar, R. Lan, C.T.G. Petit, S. Tao, Electrochemical synthesis of ammonia based on Co_3Mo_3N catalyst and $LiAlO_2$–$(Li,Na,K)_2CO_3$ composite electrolyte, Electrocatalysis 6 (2015) 286–294.
[62] I.A. Amar, R. Lan, C.T.G. Petit, S. Tao, Solid-state electrochemical synthesis of ammonia: A review, J. Solid State Electr. 15 (2011) 1845–1860.
[63] K. Kim, J.-N. Kim, H.C. Yoon, J.-I. Han, Effect of electrode material on the electrochemical reduction of nitrogen in a molten LiCl–KCl–CsCl system, Int. J. Hydrog. Energy 40 (2015) 5578–5582.
[64] S. Licht, B. Cui, B. Wang, F.-F. Li, J. Lau, S. Liu, Ammonia synthesis by N_2 and steam electrolysis in molten hydroxide suspensions of nanoscale Fe_2O_3, Science 345 (2014) 637–640.
[65] K. Imamura, J. Kubota, Electrochemical membrane cell for NH_3 synthesis from N_2 and H_2O by electrolysis at 200 to 250 °c using a Ru catalyst, hydrogen-permeable Pd membrane and phosphate-based electrolyte, Sustain, Energy Fuels 2 (2018) 1278–1286.
[66] X. Cui, C. Tang, Q. Zhang, A review of electrocatalytic reduction of dinitrogen to ammonia under ambient conditions, Adv. Energy Mater. 8 (2018) 1800369.
[67] H.-L. Du, M. Chatti, R.Y. Hodgetts, P.V. Cherepanov, C.K. Nguyen, K. Matuszek, D.R. MacFarlane, A.N. Simonov, Electroreduction of nitrogen at almost 100% current-to-ammonia efficiency, Nature 609 (2022) 722–727.
[68] L. Li, C. Tang, H. Jin, K. Davey, S.-Z. Qiao, Main-group elements boost electrochemical nitrogen fixation, Chem 7 (2021) 3232–3255.
[69] A. Tsuneto, A. Kudo, T. Sakata, Efficient electrochemical reduction of N_2 to NH_3 catalyzed by Lithium, Chem. Lett. 22 (1993) 851–854.
[70] L. Li, C. Tang, X. Cui, Y. Zheng, X. Wang, H. Xu, S. Zhang, T. Shao, K. Davey, S.-Z. Qiao, Efficient nitrogen fixation to ammonia through integration of plasma oxidation with electrocatalytic reduction, Angew. Chem. Int. Ed. 60 (2021) 14131–14137.
[71] S.-L. Meng, C. Zhang, C. Ye, J.-H. Li, S. Zhou, L. Zhu, X.-B. Li, C.-H. Tung, L.-Z. Wu, Cobaloximes: Selective nitrite reduction catalysts for tandem ammonia synthesis, Energy Environ. Sci. 16 (2023) 1590–1596.
[72] Y. Ren, C. Yu, L. Wang, X. Tan, Z. Wang, Q. Wei, Y. Zhang, J. Qiu, Microscopic-level insights into the mechanism of enhanced NH_3 synthesis in plasma-enabled cascade N_2 oxidation–electroreduction system, J. Am. Chem. Soc. 144 (2022) 10193–10200.
[73] M.M.M. Kuypers, H.K. Marchant, B. Kartal, The microbial nitrogen-cycling network, Nat. Rev. Microbiol. 16 (2018) 263–276.
[74] P.H. van Langevelde, I. Katsounaros, M.T.M. Koper, Electrocatalytic nitrate reduction for sustainable ammonia production, Joule 5 (2021) 290–294.
[75] Y. Yu, C. Wang, Y. Yu, Y. Wang, B. Zhang, Promoting selective electroreduction of nitrates to ammonia over electron-deficient Co modulated by rectifying schottky contacts, Sci. China Chem. 63 (2020) 1469–1476.
[76] T. Ren, K. Ren, M. Wang, M. Liu, Z. Wang, H. Wang, X. Li, L. Wang, Y. Xu, Concave-convex surface oxide layers over copper nanowires boost electrochemical nitrate-to-ammonia conversion, Chem. Eng. J. 426 (2021), 130759.
[77] Y. Xu, Y. Wen, T. Ren, H. Yu, K. Deng, Z. Wang, X. Li, L. Wang, H. Wang, Engineering the surface chemical microenvironment over CuO nanowire arrays by polyaniline modification for efficient ammonia electrosynthesis from nitrate, Appl. Catal. B Environ. 320 (2023), 121981.
[78] A. Thornton, P. Pearce, S.A. Parsons, Ammonium removal from solution using ion exchange on to mesolite, an equilibrium study, J. Hazard. Mater. 147 (2007) 883–889.
[79] I. Ozturk, M. Altinbas, I. Koyuncu, O. Arikan, C. Gomec-Yangin, Advanced physico-chemical treatment experiences on young municipal landfill leachates, Waste Manag. 23 (2003) 441–446.
[80] Y. Wang, W. Zhou, R. Jia, Y. Yu, B. Zhang, Unveiling the activity origin of a copper-based electrocatalyst for selective nitrate reduction to ammonia, Angew. Chem. Int. Ed. 59 (2020) 5350–5354.
[81] Y. Wang, C. Wang, M. Li, Y. Yu, B. Zhang, Nitrate electroreduction: Mechanism insight, in situ characterization, performance evaluation, and challenges, Chem. Soc. Rev. 50 (2021) 6720–6733.
[82] M.T. de Groot, M.T.M. Koper, The influence of nitrate concentration and acidity on the electrocatalytic reduction of nitrate on platinum, J. Electroanal. Chem. 562 (2004) 81–94.
[83] S. Garcia-Segura, M. Lanzarini-Lopes, K. Hristovski, P. Westerhoff, Electrocatalytic reduction of nitrate: Fundamentals to full-scale water treatment applications, Appl. Catal. B Environ. 236 (2018) 546–568.
[84] X. Zhang, Y. Wang, Y. Wang, Y. Guo, X. Xie, Y. Yu, B. Zhang, Recent advances in electrocatalytic nitrite reduction, Chem. Commun. 58 (2022) 2777–2787.
[85] X. Zhu, X. Fan, H. Lin, S. Li, Q. Zhai, Y. Jiang, Y. Chen, Highly efficient electroenzymatic cascade reduction reaction for the conversion of nitrite to ammonia, Adv. Energy Mater. 13 (2023) 2300669.
[86] J. Yuan, H. Yin, X. Jin, D. Zhao, Y. Liu, A. Du, X. Liu, A.P. O'Mullane, A practical FeP nanoarrays electrocatalyst for efficient catalytic reduction of nitrite ions in wastewater to ammonia, Appl. Catal. B Environ. 325 (2023), 122353.
[87] G. Yang, P. Zhou, J. Liang, H. Li, F. Wang, Opportunities and challenges in aqueous nitrate and nitrite reduction beyond electrocatalysis, Inorg. Chem. Front. 10 (2023) 4610–4631.
[88] Y. Li, C. Cheng, S. Han, Y. Huang, X. Du, B. Zhang, Y. Yu, Electrocatalytic reduction of low-concentration nitric oxide into ammonia over ru nanosheets, ACS Energy Lett. 7 (2022) 1187–1194.
[89] Y. Liu, Z. Liu, C. Wang, J. Xu, J. Ai, X. Liu, A. Zhang, Y. Zhao, C. Du, B. Shan, Unraveling the lattice O assisted internal selective catalytic reduction mechanism on high N_2 selectivity of CuO_x/PtCu catalysts in NH_3-SCO, ACS Catal. 13 (2023) 7178–7188.
[90] J. Long, S. Chen, Y. Zhang, C. Guo, X. Fu, D. Deng, J. Xiao, Direct electrochemical ammonia synthesis from nitric oxide, Angew. Chem. Int. Ed. 59 (2020) 9711–9718.
[91] T. Wu, W. Fan, Y. Zhang, F. Zhang, Electrochemical synthesis of ammonia: Progress and challenges, Mater. Today Phys. 16 (2021), 100310.
[92] C. He, H. Yang, M. Xi, L. Fu, J. Huo, C. Zhao, Efficient electrocatalytic reduction of NO to ammonia on BC_3 nanosheets, Environ. Res. 212 (2022), 113479.
[93] A.J. Martín, F.L.P. Veenstra, J. Lüthi, R. Verel, J. Pérez-Ramírez, Toward reliable and accessible ammonia quantification in the electrocatalytic reduction of nitrogen, Chem. Catal. 1 (2021) 1505–1518.
[94] Z. Genfa, P.K. Dasgupta, Fluorometric measurement of aqueous ammonium ion in a flow injection system, Anal. Chem. 61 (1989) 408–412.
[95] N. Amornthammarong, J.-Z. Zhang, Shipboard fluorometric flow analyzer for high-resolution underway measurement of ammonium in seawater, Anal. Chem. 80 (2008) 1019–1026.
[96] K.-i Aika, T. Takano, S. Murata, Preparation and characterization of chlorine-free ruthenium catalysts and the promoter effect in ammonia synthesis: 3. A magnesia-supported ruthenium catalyst, J. Catal. 136 (1992) 126–140.
[97] E.W. Rice, R.B. Baird, A.D. Eaton, L.S. Clesceri, Standard methods for the examination of water and wastewater, American water works association, 22 ed., 2012.
[98] G.G. Guilbault, Use of enzymes in analytical chemistry, Anal. Chem. 38 (1966) 527–536.
[99] A. Vanselow, Preparation of nessler's reagent, Ind. Eng. Chem. Anal. Ed. 12 (1940) 516–517.
[100] P.L. Searle, The berthelot or indophenol reaction and its use in the analytical chemistry of nitrogen, A Rev., Anal. 109 (1984) 549–568.
[101] B.L. Hampson, The analysis of ammonia in polluted sea water, Water Res 11 (1977) 305–308.
[102] L. SolÓRzano, Determination of ammonia in natural waters by the phenolhypochlorite method, Limnol. Oceanogr. 14 (1969) 799–801.
[103] K. Grasshoff, H. Johannsen, A new sensitive and direct method for the automatic determination of ammonia in sea water, ICES J. Mar. Sci. 34 (1972) 516–521.
[104] I. Ivančič, D. Degobbis, An optimal manual procedure for ammonia analysis in natural waters by the indophenol blue method, Water Res 18 (1984) 1143–1147.
[105] N.M. Tzollas, G.A. Zachariadis, A.N. Anthemidis, J.A. Stratis, A new approach to indophenol blue method for determination of ammonium in geothermal waters with high mineral content, Int. J. Environ. Chem. 90 (2010) 115–126.
[106] J. Reardon, J.A. Foreman, R.L. Searcy, New reactants for the colorimetric determination of ammonia, Clin. Chim. Acta 14 (1966) 403–405.
[107] H. Verdouw, C.J.A. Van Echteld, E.M.J. Dekkers, Ammonia determination based on indophenol formation with sodium salicylate, Water Res 12 (1978) 399–402.
[108] D.H. Thomas, M. Rey, P.E. Jackson, Determination of inorganic cations and ammonium in environmental waters by ion chromatography with a high-capacity cation-exchange column, J. Chromatogr. A 956 (2002) 181–186.
[109] Y. Zhao, F. Wu, Y. Miao, C. Zhou, N. Xu, R. Shi, L.-Z. Wu, J. Tang, T. Zhang, Revealing ammonia quantification minefield in photo/electrocatalysis, Angew. Chem. Int. Ed. 60 (2021) 21728–21731.
[110] R. Michalski, Applications of ion chromatography for the determination of inorganic cations, Crit. Rev. Anal. Chem. 39 (2009) 230–250.
[111] G.Y. Duan, Y. Ren, Y. Tang, Y.Z. Sun, Y.M. Chen, P.Y. Wan, X.J. Yang, Improving the reliability and accuracy of ammonia quantification in electro- and photochemical synthesis, ChemSusChem 13 (2020) 88–96.
[112] L. Zhou, C.E. Boyd, Comparison of nessler, phenate, salicylate and ion selective electrode procedures for determination of total ammonia nitrogen in aquaculture, Aquaculture 450 (2016) 187–193.
[113] B.H.R. Suryanto, H.-L. Du, D. Wang, J. Chen, A.N. Simonov, D.R. MacFarlane, Challenges and prospects in the catalysis of electroreduction of nitrogen to ammonia, Nat. Catal. 2 (2019) 290–296.
[114] L. Zhang, L.-X. Ding, G.-F. Chen, X. Yang, H. Wang, Ammonia synthesis under ambient conditions: Selective electroreduction of dinitrogen to ammonia on black phosphorus nanosheets, Angew. Chem. Int. Ed. 58 (2019) 2612–2616.
[115] S.Z. Andersen, V. Čolić, S. Yang, J.A. Schwalbe, A.C. Nielander, J.M. McEnaney, K. Enemark-Rasmussen, J.G. Baker, A.R. Singh, B.A. Rohr, M.J. Statt, S.J. Blair, S. Mezzavilla, J. Kibsgaard, P.C.K. Vesborg, M. Cargnello, S.F. Bent, T. F. Jaramillo, I.E.L. Stephens, J.K. Nørskov, I. Chorkendorff, A rigorous electrochemical ammonia synthesis protocol with quantitative isotope measurements, Nature 570 (2019) 504–508.
[116] M.Y. Masoomi, A. Morsali, A. Dhakshinamoorthy, H. Garcia, Mixed-metal MOFs: Unique opportunities in metal–organic framework (MOF) functionality and design, Angew. Chem. Int. Ed. 58 (2019) 15188–15205.
[117] Q. Wang, D. Astruc, State of the art and prospects in metal–organic framework (MOF)-based and MOF-derived nanocatalysis, Chem. Rev. 120 (2020) 1438–1511.
[118] H. Furukawa, K.E. Cordova, M. O'Keeffe, O.M. Yaghi, The chemistry and applications of metal-organic frameworks, Science 341 (2013) 1230444.

[119] X.F. Lu, B.Y. Xia, S.-Q. Zang, X.W. Lou, Metal–organic frameworks based electrocatalysts for the oxygen reduction reaction, Angew. Chem. Int. Ed. 59 (2020) 4634–4650.
[120] G. Xu, C. Zhu, G. Gao, Recent progress of advanced conductive metal–organic frameworks: Precise synthesis, electrochemical energy storage applications, and future challenges, Small 18 (2022) 2203140.
[121] B. He, Q. Zhang, Z. Pan, L. Li, C. Li, Y. Ling, Z. Wang, M. Chen, Z. Wang, Y. Yao, Q. Li, L. Sun, J. Wang, L. Wei, Freestanding metal–organic frameworks and their derivatives: An emerging platform for electrochemical energy storage and conversion, Chem. Rev. 122 (2022) 10087–10125.
[122] J.-D. Yi, D.-H. Si, R. Xie, Q. Yin, M.-D. Zhang, Q. Wu, G.-L. Chai, Y.-B. Huang, R. Cao, Conductive two-dimensional phthalocyanine-based metal–organic framework nanosheets for efficient electroreduction of CO_2, Angew. Chem. Int. Ed. 60 (2021) 17108–17114.
[123] M.-D. Zhang, D.-H. Si, J.-D. Yi, S.-S. Zhao, Y.-B. Huang, R. Cao, Conductive phthalocyanine-based covalent organic framework for highly efficient electroreduction of carbon dioxide, Small 16 (2020) 2005254.
[124] Y. Huang, S.L. Zhang, X.F. Lu, Z.-P. Wu, D. Luan, X.W. Lou, Trimetallic spinel $NiCo_{2-x}Fe_xO_4$ nanoboxes for highly efficient electrocatalytic oxygen evolution, Angew. Chem. Int. Ed. 60 (2021) 11841–11846.
[125] Y. Huang, Y. Fang, X.F. Lu, D. Luan, X.W. Lou, Co_3O_4 hollow nanoparticles embedded in mesoporous walls of carbon nanoboxes for efficient lithium storage, Angew. Chem. Int. Ed. 59 (2020) 19914–19918.
[126] J. Zhang, H. Zhang, Y. Wu, C. Liu, Y. Huang, W. Zhou, B. Zhang, Single-atom catalysts for thermal- and electro-catalytic hydrogenation reactions, J. Mater. Chem. A 10 (2022) 5743–5757.
[127] Z. Wang, M. Cheng, Y. Liu, Z. Wu, H. Gu, Y. Huang, L. Zhang, X. Liu, Dual-atomic-site catalysts for molecular oxygen activation in heterogeneous thermo-/electro-catalysis, Angew. Chem. Int. Ed. 62 (2023), e202301483.
[128] Z.-J. Lin, J. Lü, M. Hong, R. Cao, Metal–organic frameworks based on flexible ligands (FL-MOFs): Structures and applications, Chem. Soc. Rev. 43 (2014) 5867–5895.
[129] S. Wang, C.M. McGuirk, A. d'Aquino, J.A. Mason, C.A. Mirkin, Metal–organic framework nanoparticles, Adv. Mater. 30 (2018) 1800202.
[130] J.-R. Li, J. Sculley, H.-C. Zhou, Metal–organic frameworks for separations, Chem. Rev. 112 (2012) 869–932.
[131] J. Lee, O.K. Farha, J. Roberts, K.A. Scheidt, S.T. Nguyen, J.T. Hupp, Metal–organic framework materials as catalysts, Chem. Soc. Rev. 38 (2009) 1450–1459.
[132] S. Dhaka, R. Kumar, A. Deep, M.B. Kurade, S.-W. Ji, B.-H. Jeon, Metal–organic frameworks (MOFs) for the removal of emerging contaminants from aquatic environments, Coord. Chem. Rev. 380 (2019) 330–352.
[133] P.-Q. Liao, J.-Q. Shen, J.-P. Zhang, Metal–organic frameworks for electrocatalysis, Coord. Chem. Rev. 373 (2018) 22–48.
[134] N.F. Suremann, B.D. McCarthy, W. Gschwind, A. Kumar, B.A. Johnson, L. Hammarström, S. Ott, Molecular catalysis of energy relevance in metal–organic frameworks: From higher coordination sphere to system effects, Chem. Rev. 123 (2023) 6545–6611.
[135] H.-D. Lim, B. Lee, Y. Bae, H. Park, Y. Ko, H. Kim, J. Kim, K. Kang, Reaction chemistry in rechargeable Li–O_2 batteries, Chem. Soc. Rev. 46 (2017) 2873–2888.
[136] J. Zhou, B. Wang, Emerging crystalline porous materials as a multifunctional platform for electrochemical energy storage, Chem. Soc. Rev. 46 (2017) 6927–6945.
[137] G. Zhou, B. Wang, R. Cao, Acid catalysis in confined channels of metal–organic frameworks: Boosting orthoformate hydrolysis in basic solutions, J. Am. Chem. Soc. 142 (2020) 14848–14853.
[138] A. Jain, R. Balasubramanian, M.P. Srinivasan, Hydrothermal conversion of biomass waste to activated carbon with high porosity: A review, Chem. Eng. J. 283 (2016) 789–805.
[139] L. Chen, H.-F. Wang, C. Li, Q. Xu, Bimetallic metal–organic frameworks and their derivatives, Chem. Sci. 11 (2020) 5369–5403.
[140] S. Kitagawa, R. Kitaura, S.-i Noro, Functional porous coordination polymers, Angew. Chem. Int. Ed. 43 (2004) 2334–2375.
[141] B. Zhu, Z. Liang, D. Xia, R. Zou, Metal-organic frameworks and their derivatives for metal-air batteries, Energy Storage Mater. 23 (2019) 757–771.
[142] W. Xia, A. Mahmood, R. Zou, Q. Xu, Metal–organic frameworks and their derived nanostructures for electrochemical energy storage and conversion, Energy Environ. Sci. 8 (2015) 1837–1866.
[143] T. Hu, L. Tang, H. Feng, J. Zhang, X. Li, Y. Zuo, Z. Lu, W. Tang, Metal-organic frameworks (MOFs) and their derivatives as emerging catalysts for electro-Fenton process in water purification, Coord. Chem. Rev. 451 (2022), 214277.
[144] Y.-S. Wei, L. Zou, H.-F. Wang, Y. Wang, Q. Xu, Micro/nano-scaled metal-organic frameworks and their derivatives for energy applications, Adv. Energy Mater. 12 (2022) 2003970.
[145] G. Yilmaz, S.B. Peh, D. Zhao, G.W. Ho, Atomic- and molecular-level design of functional metal–organic frameworks (MOFs) and derivatives for energy and environmental applications, Adv. Sci. 6 (2019) 1901129.
[146] M. Shen, H. Ma, Metal-organic frameworks (MOFs) and their derivative as electrode materials for lithium-ion batteries, Coord. Chem. Rev. 470 (2022), 214715.
[147] S. Fu, C. Zhu, J. Song, D. Du, Y. Lin, Metal-organic framework-derived non-precious metal nanocatalysts for oxygen reduction reaction, Adv. Energy Mater. 7 (2017) 1700363.
[148] Z. Liang, T. Qiu, S. Gao, R. Zhong, R. Zou, Multi-scale design of metal–organic framework-derived materials for energy electrocatalysis, Adv. Energy Mater. 12 (2022) 2003410.
[149] T. De Villenoisy, X. Zheng, V. Wong, S.S. Mofarah, H. Arandiyan, Y. Yamauchi, P. Koshy, C.C. Sorrell, Principles of design and synthesis of metal derivatives from MOFs, Adv. Mater. 35 (2023) 2210166.
[150] W. Xue, Q. Zhou, X. Cui, S. Jia, J. Zhang, Z. Lin, Metal–organic frameworks-derived heteroatom-doped carbon electrocatalysts for oxygen reduction reaction, Nano Energy 86 (2021), 106073.
[151] Y. Sun, B. Xia, S. Ding, L. Yu, S. Chen, J. Duan, Rigid two-dimensional indium metal–organic frameworks boosting nitrogen electroreduction at all pH values, J. Mater. Chem. A 9 (2021) 20040–20047.
[152] J. Duan, Y. Sun, S. Chen, X. Chen, C. Zhao, A zero-dimensional nickel, iron–metal–organic framework (MOF) for synergistic N_2 electrofixation, J. Mater. Chem. A 8 (2020) 18810–18815.
[153] H. He, Q.-Q. Zhu, Y. Yan, H.-W. Zhang, Z.-Y. Han, H. Sun, J. Chen, C.-P. Li, Z. Zhang, M. Du, Metal–organic framework supported Au nanoparticles with organosilicone coating for high-efficiency electrocatalytic N_2 reduction to NH_3, Appl. Catal. B Environ. 302 (2022), 120840.
[154] H.Y.F. Sim, J.R.T. Chen, C.S.L. Koh, H.K. Lee, X. Han, G.C. Phan-Quang, J.Y. Pang, C.L. Lay, S. Pedireddy, I.Y. Phang, E.K.L. Yeow, X.Y. Ling, ZIF-induced d-band modification in a bimetallic nanocatalyst: Achieving over 44% efficiency in the ambient nitrogen reduction reaction, Angew. Chem. Int. Ed. 59 (2020) 16997–17003.
[155] H.K. Lee, C.S.L. Koh, Y.H. Lee, C. Liu, I.Y. Phang, X. Han, C.-K. Tsung, X.Y. Ling, Favoring the unfavored: Selective electrochemical nitrogen fixation using a reticular chemistry approach, Sci. Adv. 4 (2018) eaar3208.
[156] X. Liang, X. Ren, Q. Yang, L. Gao, M. Gao, Y. Yang, H. Zhu, G. Li, T. Ma, A. Liu, A two-dimensional Mxene-supported metal-organic framework for highly selective ambient electrocatalytic nitrogen reduction, Nanoscale 13 (2021) 2843–2848.
[157] J. Duan, D. Shao, X. He, Y. Lu, W. Wang, Model MoS_2@ZIF-71 interface acts as a highly active and selective electrocatalyst for catalyzing ammonia synthesis, Colloids Surf. A Physicochem. Eng. Asp. 619 (2021), 126529.
[158] Y. Lv, Y. Wang, M. Yang, Z. Mu, S. Liu, W. Ding, M. Ding, Nitrogen reduction through confined electro-catalysis with carbon nanotube inserted metal–organic frameworks, J. Mater. Chem. A 9 (2021) 1480–1486.
[159] W.-Y. Xu, C. Li, F.-L. Li, J.-Y. Xue, W. Zhang, H. Gu, B.F. Abrahams, J.-P. Lang, A hybrid catalyst for efficient electrochemical N_2 fixation formed by decorating amorphous MoS_3 nanosheets with MIL-101(Fe) nanodots, Sci. China Chem. 65 (2022) 885–891.
[160] L. Wen, K. Sun, X. Liu, W. Yang, L. Li, H.-L. Jiang, Electronic state and microenvironment modulation of metal nanoparticles stabilized by MOFs for boosting electrocatalytic nitrogen reduction, Adv. Mater. 35 (2023) 2210669.
[161] W. Li, W. Fang, C. Wu, K.N. Dinh, H. Ren, L. Zhao, C. Liu, Q. Yan, Bimetal–MOF nanosheets as efficient bifunctional electrocatalysts for oxygen evolution and nitrogen reduction reaction, J. Mater. Chem. A 8 (2020) 3658–3666.
[162] X. He, F. Yin, X. Yi, T. Yang, B. Chen, X. Wu, S. Guo, G. Li, Z. Li, Defective UIO-66-NH_2 functionalized with stable superoxide radicals toward electrocatalytic nitrogen reduction with high faradaic efficiency, ACS Appl. Mater. Interfaces 14 (2022) 26571–26586.
[163] G. Deng, T. Wang, A.A. Alshehri, K.A. Alzahrani, Y. Wang, H. Ye, Y. Luo, X. Sun, Improving the electrocatalytic N_2 reduction activity of Pd nanoparticles through surface modification, J. Mater. Chem. A 7 (2019) 21674–21677.
[164] M. Cong, X. Chen, K. Xia, X. Ding, L. Zhang, Y. Jin, Y. Gao, L. Zhang, Selective nitrogen reduction to ammonia on iron porphyrin-based single-site metal–organic frameworks, J. Mater. Chem. A 9 (2021) 4673–4678.
[165] P. Liu, P. Jing, X. Xu, B. Liu, J. Zhang, Structural reconstruction of Ce-MOF with active sites for efficient electrocatalytic N_2 reduction, ACS Appl. Energy Mater. 4 (2021) 12128–12136.
[166] Y. Fu, K. Li, M. Batmunkh, H. Yu, S. Donne, B. Jia, T. Ma, Unsaturated p-metal-based metal–organic frameworks for selective nitrogen reduction under ambient conditions, ACS Appl. Mater. Interfaces 12 (2020) 44830–44839.
[167] X. Zhu, H. Huang, H. Zhang, Y. Zhang, P. Shi, K. Qu, S.B. Cheng, A.L. Wang, Q. Lu, Filling mesopores of conductive metal-organic frameworks with Cu clusters for selective nitrate reduction to ammonia, ACS Appl. Mater. Interfaces 14 (2022) 32176–32182.
[168] J. Ma, Y. Zhang, B. Wang, Z. Jiang, Q. Zhang, S. Zhuo, Interfacial engineering of bimetallic Ni/Co-MOFs with H-substituted graphdiyne for ammonia electrosynthesis from nitrate, ACS Nano 17 (2023) 6687–6697.
[169] J. Ma, R. Wang, B. Wang, J. Luo, Q. Zhang, S. Zhuo, Hybrid nanoarrays of Cu-MOFs@H-substituted graphdiyne with various levels of lewis acidity for nitrate electroreduction, Chem. Commun. 59 (2023) 4348–4351.
[170] M. Jiang, J. Su, X. Song, P. Zhang, M. Zhu, L. Qin, Z. Tie, J.-L. Zuo, Z. Jin, Interfacial reduction nucleation of noble metal nanodots on redox-active metal–organic frameworks for high-efficiency electrocatalytic conversion of nitrate to ammonia, Nano Lett. 22 (2022) 2529–2537.
[171] J. Qin, K. Wu, L. Chen, X. Wang, Q. Zhao, B. Liu, Z. Ye, Achieving high selectivity for nitrate electrochemical reduction to ammonia over MOF-supported Ru_xO_y clusters, J. Mater. Chem. A 10 (2022) 3963–3969.
[172] Y. Lv, S.-W. Ke, Y. Gu, B. Tian, L. Tang, P. Ran, Y. Zhao, J. Ma, J.-L. Zuo, M. Ding, Highly efficient electrochemical nitrate reduction to ammonia in strong acid conditions with Fe_2M-Trinuclear-Cluster metal–organic frameworks, Angew. Chem. Int. Ed. 62 (2023), e202305246.
[173] Z. Wang, S. Liu, M. Wang, L. Zhang, Y. Jiang, T. Qian, J. Xiong, C. Yang, C. Yan, In situ construction of metal–organic frameworks as smart channels for the effective electrocatalytic reduction of nitrate at ultralow concentrations to ammonia, ACS Catal. 13 (2023) 9125–9135.

[174] Z. Feng, Z. Yang, X. Meng, F. Li, Z. Guo, S. Zheng, G. Su, Y. Ma, Y. Tang, X. Dai, Two-dimensional metal–organic framework $Mo_3(C_2O)_{12}$ as a promising single-atom catalyst for selective nitrogen-to-ammonia conversion, J. Mater. Chem. A 10 (2022) 4731–4738.
[175] Y. Liu, C. Li, L. Guan, K. Li, Y. Lin, Oxygen vacancy regulation strategy promotes electrocatalytic nitrogen fixation by doping Bi into Ce-MOF-derived CeO_2 nanorods, J. Phys. Chem. C. 124 (2020) 18003–18009.
[176] X. Zhao, F. Yin, N. Liu, G. Li, T. Fan, B. Chen, Highly efficient metal–organic-framework catalysts for electrochemical synthesis of ammonia from N_2 (air) and water at low temperature and ambient pressure, J. Mater. Sci. 52 (2017) 10175–10185.
[177] B. Li, W. Du, Q. Wu, Y. Dai, B. Huang, Y. Ma, Coronene-based 2D metal–organic frameworks: A new family of promising single-atom catalysts for nitrogen reduction reaction, J. Phys. Chem. C. 125 (2021) 20870–20876.
[178] R. Wang, C. He, W. Chen, L. Fu, C. Zhao, J. Huo, C. Sun, Design strategies of two-dimensional metal–organic frameworks toward efficient electrocatalysts for N_2 reduction: Cooperativity of transition metals and organic linkers, Nanoscale 13 (2021) 19247–19254.
[179] X. Xin, Q. Qu, I.E. Khalil, Y. Huang, M. Wei, J. Chen, W. Zhang, F. Huo, W. Liu, Hetero-phase zirconia encapsulated with Au nanoparticles for boosting electrocatalytic nitrogen reduction, Chin. Chem. Lett. (2023), 108654.
[180] K.-Y. Hsiao, Y.-H. Tseng, C.-L. Chiang, Y.-D. Chen, Y.-G. Lin, M.-Y. Lu, Environment-dependent structural evolution and electrocatalytic performance in N_2 reduction of Mo-based ZIF-8, ACS Appl. Nano Mater. 6 (2023) 10713–10724.
[181] X. Liang, X. Ren, Q. Yang, L. Gao, M. Gao, Y. Yang, H. Zhu, G. Li, T. Ma, A. Liu, A two-dimensional mxene-supported metal–organic framework for highly selective ambient electrocatalytic nitrogen reduction, Nanoscale 13 (2021) 2843–2848.
[182] H. Huang, Q. Liu, Q. Cheng, M. Zhang, J. Liu, Incorporating Pd into Cu-coordinated metal-organic frameworks to promote N_2 electrochemical reduction into ammonia, ChemCatChem 14 (2022), e202201114.
[183] J. Cao, Z. Yang, W. Xiong, Y. Zhou, Y. Wu, M. Jia, C. Zhou, Z. Xu, Ultrafine metal species confined in metal–organic frameworks: Fabrication, characterization and photocatalytic applications, Coord. Chem. Rev. 439 (2021), 213924.
[184] B. Huang, B. Chen, G. Zhu, J. Peng, P. Zhang, Y. Qian, N. Li, Electrochemical ammonia synthesis via NO reduction on 2D-MOF, ChemPhysChem 23 (2022), e202100785.
[185] J. Wang, H. Huang, P. Wang, S. Wang, J. Li, N, s synergistic effect in hierarchical porous carbon for enhanced nrr performance, Carbon 179 (2021) 358–364.
[186] F. Yin, X. Lin, X. He, B. Chen, G. Li, H. Yin, High faraday efficiency for electrochemical nitrogen reduction reaction on Co@N-doped carbon derived from a metal-organic framework under ambient conditions, Mater. Lett. 248 (2019) 109–113.
[187] Z. Zhang, K. Yao, L. Cong, Z. Yu, L. Qu, W. Huang, Facile synthesis of a Ru-dispersed N-doped carbon framework catalyst for electrochemical nitrogen reduction, Catal. Sci. Technol. 10 (2020) 1336–1342.
[188] C. Ma, D. Liu, Y. Zhang, J. Yong Lee, J. Tian, B. Liu, S. Yan, MOF-derived Fe_2O_3@MoS_2: An efficient electrocatalyst for ammonia synthesis under mild conditions, Chem. Eng. J. 430 (2022), 132694.
[189] L. Cong, K. Yao, S. Zhang, Z. Zhang, Z. Yu, M. Qian, L. Qu, W. Huang, Facile synthesis of bimetallic N-doped carbon hybrid material for electrochemical nitrogen reduction, J. Energy Chem. 59 (2021) 715–720.
[190] B. Yan, S. Hu, C. Bu, Ya Peng, H. Han, X. Xu, Y. Liu, J. Yu, Y. Dai, TiO_2/CeO_2 frame with enriched oxygen vacancies and Hetero-interfaces for efficient electrochemical N_2 reduction, ChemCatChem 15 (2023), e202300076.
[191] Z. Geng, Y. Liu, X. Kong, P. Li, K. Li, Z. Liu, J. Du, M. Shu, R. Si, J. Zeng, Achieving a record-high yield rate of 120.9 for N_2 electrochemical reduction over Ru single-atom catalysts, Adv. Mater. 30 (2018) 1803498.
[192] R. Zhang, L. Jiao, W. Yang, G. Wan, H.-L. Jiang, Single-atom catalysts templated by metal–organic frameworks for electrochemical nitrogen reduction, J. Mater. Chem. A 7 (2019) 26371–26377.
[193] S. Chen, H. Jang, J. Wang, Q. Qin, X. Liu, J. Cho, Bimetallic metal–organic framework-derived mofe-pc microspheres for electrocatalytic ammonia synthesis under ambient conditions, J. Mater. Chem. A 8 (2020) 2099–2104.
[194] Y. Zhang, J. Hu, C. Zhang, Y. Liu, M. Xu, Y. Xue, L. Liu, M.K.H. Leung, Bimetallic Mo–Co nanoparticles anchored on nitrogen-doped carbon for enhanced electrochemical nitrogen fixation, J. Mater. Chem. A 8 (2020) 9091–9098.
[195] Q. Qin, Y. Zhao, M. Schmallegger, T. Heil, J. Schmidt, R. Walczak, G. Gescheidt-Demner, H. Jiao, M. Oschatz, Enhanced electrocatalytic N_2 reduction via partial anion substitution in titanium oxide–carbon composites, Angew. Chem. Int. Ed. 58 (2019) 13101–13106.
[196] W. Guo, Z. Liang, J. Zhao, B. Zhu, K. Cai, R. Zou, Q. Xu, Hierarchical cobalt phosphide hollow nanocages toward electrocatalytic ammonia synthesis under ambient pressure and room temperature, Small Methods 2 (2018) 1800204.
[197] S. Luo, X. Li, M. Wang, X. Zhang, W. Gao, S. Su, G. Liu, M. Luo, Long-term electrocatalytic N_2 fixation by MOF-derived Y-stabilized ZrO_2: Insight into the deactivation mechanism, J. Mater. Chem. A 8 (2020) 5647–5654.
[198] F. Lü, S. Zhao, R. Guo, J. He, X. Peng, H. Bao, J. Fu, L. Han, G. Qi, J. Luo, X. Tang, X. Liu, Nitrogen-coordinated single Fe sites for efficient electrocatalytic N_2 fixation in neutral media, Nano Energy 61 (2019) 420–427.
[199] J. Duan, D. Shao, W. Wang, D. Zhang, C. Li, Strongly coupled molybdenum phosphide@phosphorus-doped porous carbon derived from MOF used in N_2 electroreduction under ambient conditions, Micropor. Mesopor, Mater 313 (2021), 110852.
[200] J. Chen, T. Gong, Q. Hou, J. Li, L. Zhang, D. Zhao, Y. Luo, D. Zheng, T. Li, S. Sun, Z. Cai, Q. Liu, L. Xie, M. Wu, A.A. Alshehri, X. Sun, Co/N-doped carbon nanospheres derived from an adenine-based metal organic framework enabled high-efficiency electrocatalytic nitrate reduction to ammonia, Chem. Commun. 58 (2022) 13459–13462.
[201] Z. Song, Y. Liu, Y. Zhong, Q. Guo, J. Zeng, Z. Geng, Efficient electroreduction of nitrate into ammonia at ultralow concentrations via an enrichment effect, Adv. Mater. 34 (2022) 2204306.
[202] Y. Xue, Q. Yu, Q. Ma, Y. Chen, C. Zhang, W. Teng, J. Fan, W.-x Zhang, Electrocatalytic hydrogenation boosts reduction of nitrate to ammonia over single-atom Cu with Cu(I)-N_3C_1 sites, Environ. Sci. Technol. 56 (2022) 14797–14807.
[203] T. Ren, Z. Yu, H. Yu, K. Deng, Z. Wang, X. Li, H. Wang, L. Wang, Y. Xu, Interfacial polarization in metal-organic framework reconstructed Cu/Pd/CuO_x multi-phase heterostructures for electrocatalytic nitrate reduction to ammonia, Appl. Catal. B Environ. (2022), 121805.
[204] S. Han, H. Li, T. Li, F. Chen, R. Yang, Y. Yu, B. Zhang, Ultralow overpotential nitrate reduction to ammonia via a three-step relay mechanism, Nat. Catal. 6 (2023) 402–414.
[205] Y. Liu, B. Deng, K. Li, H. Wang, Y. Sun, F. Dong, Metal-organic framework derived carbon-supported bimetallic copper-nickel alloy electrocatalysts for highly selective nitrate reduction to ammonia, J. Colloid Interface Sci. 614 (2022) 405–414.
[206] Z. Ke, D. He, X. Yan, W. Hu, N. Williams, H. Kang, X. Pan, J. Huang, J. Gu, X. Xiao, Selective NO_x^- electroreduction to ammonia on isolated Ru sites, ACS Nano 17 (2023) 3483–3491.
[207] M. Xu, Q. Xie, D. Duan, Y. Zhang, Y. Zhou, H. Zhou, X. Li, Y. Wang, P. Gao, W. Ye, Atomically dispersed Cu sites on dual-mesoporous N-doped carbon for efficient ammonia electrosynthesis from nitrate, ChemSusChem 15 (2022), e202200231.
[208] Y. Wang, H. Yin, F. Dong, X. Zhao, Y. Qu, L. Wang, Y. Peng, D. Wang, W. Fang, J. Li, N-coordinated Cu–Ni dual-single-atom catalyst for highly selective electrocatalytic reduction of nitrate to ammonia, Small 19 (2023) 2207695.
[209] S. Xu, Y. Shi, Z. Wen, X. Liu, Y. Zhu, G. Liu, H. Gao, L. Sun, F. Li, Polystyrene spheres-templated mesoporous carbonous frameworks implanted with cobalt nanoparticles for highly efficient electrochemical nitrate reduction to ammonia, Appl. Catal. B Environ. 323 (2023), 122192.
[210] J. Zhou, S. Han, R. Yang, T. Li, W. Li, Y. Wang, Y. Yu, B. Zhang, Linear adsorption enables NO selective electroreduction to hydroxylamine on single Co sites, Angew. Chem. Int. Ed. 62 (2023), e202305184.
[211] Y. Liu, Y. Su, X. Quan, X. Fan, S. Chen, H. Yu, H. Zhao, Y. Zhang, J. Zhao, Facile ammonia synthesis from electrocatalytic N_2 reduction under ambient conditions on N-doped porous carbon, ACS Catal. 8 (2018) 1186–1191.
[212] P. Song, L. Kang, H. Wang, R. Guo, R. Wang, Nitrogen (N), phosphorus (P)-codoped porous carbon as a metal-free electrocatalyst for N_2 reduction under ambient conditions, ACS Appl. Mater. Interfaces 11 (2019) 12408–12414.
[213] X. Zhang, Y. Wang, C. Liu, Y. Yu, S. Lu, B. Zhang, Recent advances in non-noble metal electrocatalysts for nitrate reduction, Chem. Eng. J. 403 (2021), 126269.